Author:
Young, Kester E J

Title:
Preserving transverse tubule function in adult cardiac myocytes in short-term culture.

Author:
Young, Kester E J

Title:
Preserving transverse tubule function in adult cardiac myocytes in short-term culture.

University of Bristol

School of Physiology, Pharmacology and Neuroscience

Preserving transverse tubule function in adult cardiac myocytes in short-term culture.

Kester Erin James Young

Supervisors: Dr Andrew James
Dr Stephen Harmer

September 2023

Abstract

T-tubules (TTs) are invaginations of sarcolemma in cardiomyocytes important in excitation-contraction coupling. Loss of TTs in short-term culture is a poorly understood phenomenon, insight into which may be valuable for development of future clinical interventions. The hypothesis that junctophilin-2 (JPH2) overexpression in adult rabbit ventricular myocytes (ARVMs) preserves TTs and calcium current (I_{Ca}) density in short-term culture was tested.

ARVMs were cultured for four days, and TT loss quantified by fast-Fourier transform analysis ('TT-power') of wheatgerm agglutinin (WGA) staining, which showed a threefold-reduction from day 0 at day 4. I_{Ca} density was obtained from whole-cell patch clamp recordings. Transduction with Ad-h-JPH2-GFP and Ad-GFP constructs was carried out at day 0 and culture media changed at day 2 of culture.

Over four days in culture ARVMs became more rounded, capacitance decreased exponentially with a time constant of 1.68 days and, by day 4, internal WGA staining was absent -indicating complete loss of TTs. At culture day 1, I_{Ca} density was half that of day 0, yet by day 4 had recovered to ~85 % of day 0. The response to 100 nM isoprenaline was preserved across days in culture. Neither TT-power nor I_{Ca} density were significantly different between day 4 ARVMs transduced with either JPH2 or GFP, and the reduction in TT-power between day 0 and day 4 was similar in JPH2-transduced (JPH2+) and non-transduced ARVMs.

Despite GFP-expression indicating successful viral transduction, JPH2-staining intensity was surprisingly low in JPH2+ ARVMs and did not correlate with GFP-intensity. Similar results were obtained from preliminary data from adult rat ventricular myocytes. In conclusion, JPH2-overexpression via Ad-h-JPH2-GFP did not lead to preservation of TTs and I_{Ca} density in ARVMs in short-term culture. However, further work is needed to quantify whether a sufficient level of JPH2-overexpression had been achieved.

Dedication and Acknowledgement

Dedication

I dedicate this thesis to my family, who have always done their best to support me.

Acknowledgements

I am extremely grateful to my supervisors, Dr Andrew James and Dr Stephen Harmer for their expert guidance, and help, and above all their unwavering patience throughout this research endeavour. I could not have done this without you.

I would very much like to thank Dr Valentina Mosienko, Dr Anja Teschemacher, Prof Sergey Kasparov and Dr Barbara V. Cardoso for training, help and advice with cell culture and imaging, virus handling and for the use of their facilities.

I would like to express my appreciation to everyone in lab C39 for always making me feel welcome and offering their help when I was faced with uncertainty. I very much enjoyed my time working with you all and wish you luck for the future.

Finally, I would like to thank the School of Physiology, Pharmacology and Neuroscience at the University of Bristol for providing the resources and conducive academic environment that facilitated this research.

Author’s Declaration

I declare that the work in this dissertation was carried out in accordance with the requirements of the University's *Regulations and Code of Practice for Research Degree Programmes* and that it has not been submitted for any other academic award. Except where indicated by specific reference in the text, the work is the candidate's own work. Work done in collaboration with, or with the assistance of, others, is indicated as such. Any views expressed in the dissertation are those of the author.

SIGNED: [redacted] DATE: 16/09/2023

Table of Contents

1. Introduction

1.1 Cardiac T-Tubules

T-tubules (TTs) are invaginations of sarcolemma that form a complex multidirectional network organised transversely within the Z groove and with longitudinal branching elements reaching into the A and I bands of the sarcomere (Figure 1) (Bers, 2008).

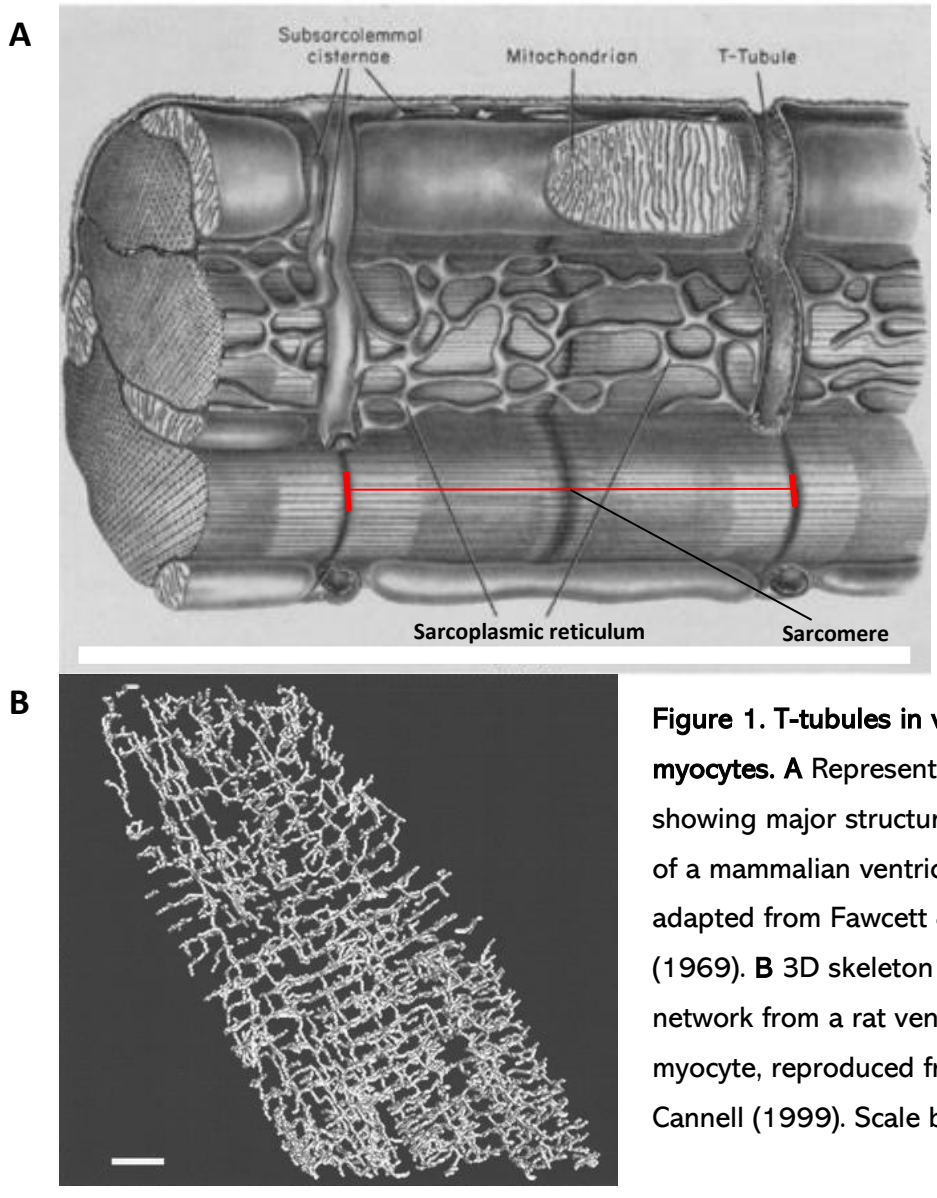

Figure 1. T-tubules in ventricular myocytes. A Representative drawing showing major structural components of a mammalian ventricular myocyte, adapted from Fawcett & McNutt (1969). **B** 3D skeleton of the T-tubule network from a rat ventricular myocyte, reproduced from Soeller & Cannell (1999). Scale bars are 5 μm.

TT membrane and junctional sarcoplasmic reticulum (SR) come together within cardiomyocytes to make up dyads – sites where calcium-induced calcium release (CICR), a process central to excitation-contraction coupling (ECC), takes place. L-type calcium channels (LTCCs) located at the t-tubular membrane and ryanodine receptors (RyRs) of the

SR constitute the functional release units of the dyad, where opening of LTCCs upon membrane depolarisation results in calcium influx into the dyadic cleft, activating RyRs which, in turn, releases calcium stored in the SR to bring about a much greater elevation in cytosolic calcium than could be achieved by opening of the LTCC alone. The 'calcium transient' represents the spatiotemporal summation of calcium release by the functional release units throughout the cell. Efficient contraction is achieved when the individual calcium release units activate in unison and the resultant large rapid increase in cytosolic calcium activates the myofilaments (Chung et al., 2016). Myofilament relaxation is achieved as calcium is sequestered back into the SR by SERCA2a or extruded from the cell, predominantly via sodium-calcium exchange (Ottolia et al., 2013).

The importance of TTs in enabling propagation of the action potential into the cell interior and thus facilitating spatiotemporal uniformity of calcium release has been well characterised (Orchard and Brette, 2008). Direct removal of TTs via osmotic shock results in a disruption to the normal process of ECC; following depolarisation-induced calcium release from coupled RyR at the cell surface, CICR propagates as a wave to the cell centre (Brette et al., 2005). Uncoupling of TTs from the cell surface has been suggested to be a potent stimulus for arrhythmia in heart tissue (Orchard et al., 2013). TTs also regulate the extracellular ionic concentration in immediate proximity to the cell (Rog-Zielinska et al., 2018, Hong et al., 2014, Kong et al., 2018b). Advancing our understanding of TT physiology in areas including TT biogenesis, the role of TTs in signalling microdomains, such as for cAMP signalling (Nikolaev et al., 2010, Gorelik et al., 2013), and TT trafficking pathways (Hong and Shaw, 2017) may lead to novel therapeutic approaches to oppose the pathological remodelling of TTs that can occur in heart disease (Guo et al., 2013, Wei et al., 2010, Crossman et al., 2015) and from aging (Kong et al., 2018a, Lyu et al., 2021).

1.2 The T-tubule network becomes disrupted in disease

Whilst many studies have identified that TT dysregulation is a common feature in heart failure (HF) it remains unclear as to whether this is a feature or a driver of the disease (Dibb et al., 2022). The importance of the ultrastructural arrangement of ventricular myocyte TTs to physiological function – particularly CICR - has long been appreciated (Soeller and Cannell, 1999) and TTs have been shown to play a key role in regulating transarcolemmal calcium flux (Brette et al., 2004b) – thus in regulating cellular calcium homeostasis. Disorder

of the calcium release process within cardiomyocytes (CMs) is a major consequence of the pathological disturbance to TT architecture in HF - tight coupling between LTCCs anchored to the TT membrane and RyRs in the SR membrane is lost. Orphaned RyRs and non-uniform CICR result, in turn promoting hypocontractility and arrhythmogenesis (Figure 2).

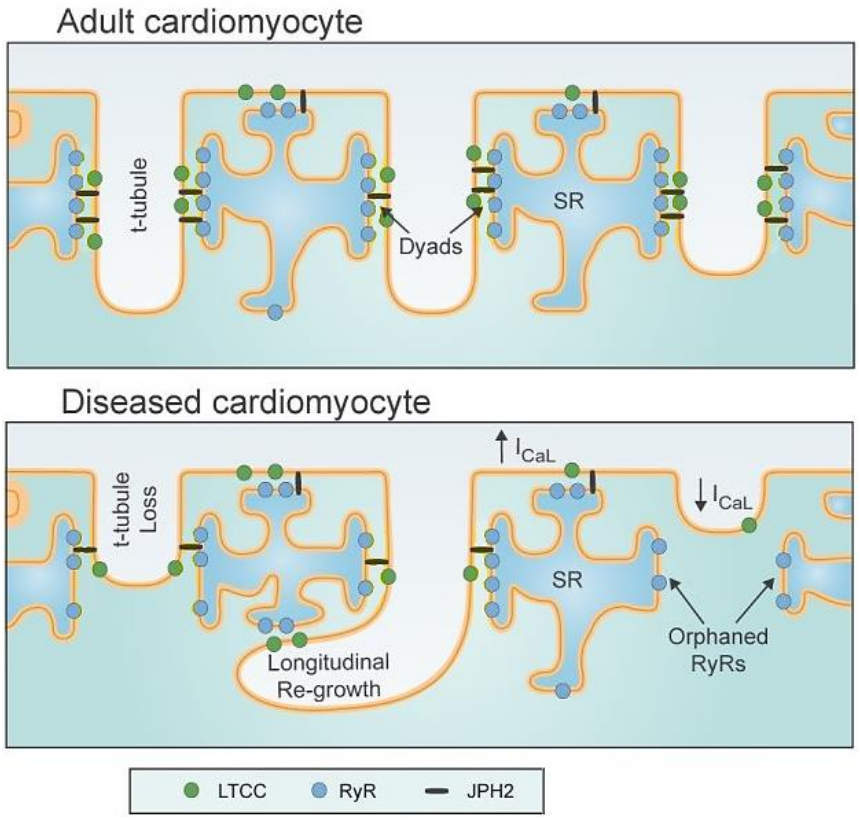

Figure 2. Regularity of T-tubules is compromised in disease. In the healthy adult cardiomyocyte T-tubules penetrate deep into the myocyte and are highly organised. In disease, T-tubules become dysregulated; most are shortened and eventually lost leading to RyRs becoming orphaned. Taken from Jones et al. (2018). RyR = ryanodine receptor; JPH2 = junctophilin 2; LTCC = L-type calcium channel; SR = sarcoplasmic reticulum.

1.3 Loss of T-tubules in cell culture

It is well established that CMs maintained in cell culture lose their TTs over time (Mitcheson et al., 1996, Mitcheson et al., 1998, Pabbathi et al., 2002, Pavlovic et al., 2010). Examining and understanding the relatively rapid cellular changes that occur during cell culture as CMs dedifferentiate (Bugaisky and Zak, 1989, Horackova and Byczko, 1997) may provide novel

and important insights into biological mechanisms that are relevant to disease (Jones et al., 2018). Indeed, several proteins have recently been shown to play important roles in stabilising TTs, in part through the use of short-term culture (Setterberg et al., 2021). One such protein, bridging-integrator 1 (Bin1), has even been suggested to promote de novo synthesis of TTs from caveolae in hiPSCs (De La Mata et al., 2019), an idea supported by a recent study in skeletal myocytes (Lemerle et al., 2023), where the authors propose tubulation stems from caveolae-Bin1 ring-shaped platforms. However, cardiac TTs remain present in the cardiac-specific Bin1 KO mouse (Hong et al., 2014) indicating, at least in cardiac myocytes, that there must be redundancy in this mechanism.

1.4 JPH2 overexpression restores TT integrity in cultured cells

The junctophillins are a family of four membrane anchoring proteins in vertebrates that are important in facilitating communication between the plasma membrane and endoplasmic reticulum (ER) or SR. These proteins have in common six membrane occupation and recognition (MORN) motifs at their N-terminus, followed by a joining region and two further MORN motifs. The C-terminal transmembrane region, which attaches to the ER/SR, is also common between isoforms and has an adjacent divergent region (Lehnart & Wehrens, 2022). Junctophillin-2 (JPH2) has garnered much interest as it has been identified as a protein intimately involved in the structural arrangement of the dyad and mutated in genetic cardiomyopathy (Takeshima et al., 2015) as well as being downregulated in HF (Jiang et al., 2016, Reynolds et al., 2016). JPH2 overexpression has also been shown to preserve TT integrity in cultured adult rat CMs (Figure 3) (Gross et al., 2021, Poulet et al., 2021) and protect against the transverse aortic constriction-induced HF phenotype (which includes TT disruption) when overexpressed in mice (Reynolds et al., 2016).

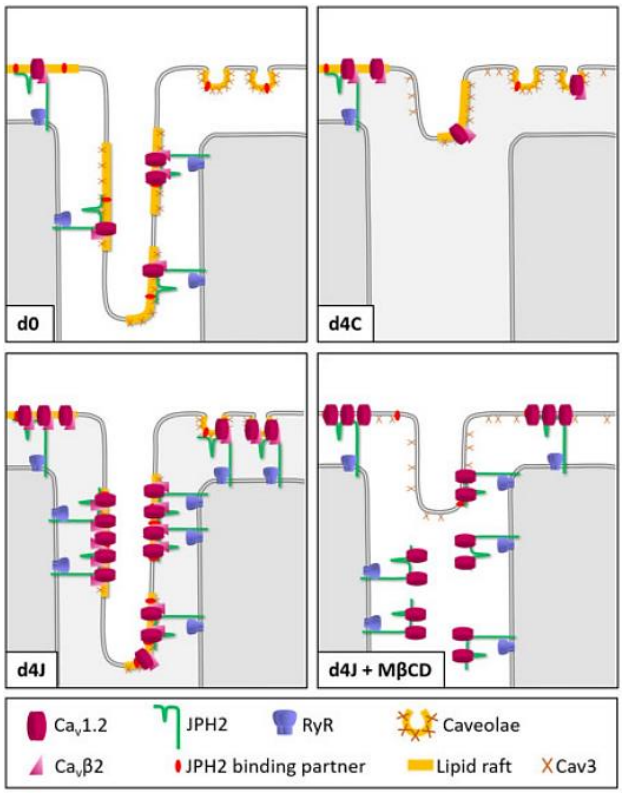

Figure 3. Cholesterol-dependent JPH2 rescue of T-tubules in adult rat ventricular myocytes. Graphical summary taken from Poulet et al. (2021) showing JPH2-supported dyads in a healthy T-tubule at day 0 of isolation (top left). At day 4 in non-transduced cells (day 4 control; d4C; top right) TTs are drastically shortened or lost. In day 4 transduced cells (day 4 junctophilin; d4J; bottom left), dyads are stabilised by excess JPH2, and this protects against loss of TTs. In the presence of the cholesterol-sequestering drug methyl-β-cyclodextrin, TTs are lost even when JPH2 is overexpressed (bottom right).

Interestingly, a recent study in hibernating ground squirrels reported an adaptive physiological mechanism of JPH2 and Cav3 upregulation via myocardin and serum response factor in response to hypothermia, identifying much stabler ECC in comparison to euthermic ground squirrels (Yang et al., 2021). Gross et al. (2021) also provide evidence from subcellular fractionation and super-resolution scanning patch clamp experiments that TT calcium release units may be preserved in JPH2-transduced CMs at day 4 of culture. These studies support the idea that JPH2 is key in stabilising TTs, preventing both remodelling and loss of LTCCs. Cav3-enriched lipid rafts and the interaction between the LTCC α1C subunit and JPH2 were also suggested to be essential in the ability of JPH2 overexpression to rescue TTs in this manner (Gross et al., 2021, Poulet et al., 2021).

1.5 Aims and Hypothesis

The present study examines the role of JPH2 in TT structure and function in adult rabbit ventricular myocytes (ARVMs) in culture, with the hypothesis that JPH2 overexpression reduces TT loss and restores LTCC current in ARVMs towards day 0 levels. Demonstrating that JPH2 effects these changes in ARVMs would add to a growing body of evidence

supporting JPH2 as a target for therapeutic approaches to prevent TT remodelling in disease.

2. Materials and Methods

2.1 Animals and cell isolation

Myocytes were isolated from the hearts of adult male New Zealand rabbits (~2.5 kg) and adult male Wistar rats (~300 g). All procedures were performed in accordance with UK legislation and approved by the University of Bristol Animal Welfare and Ethics Review Board. Animals were subject to pentobarbital anaesthesia, the heart excised and cannulated via the aorta onto a Langendorff apparatus. Myocytes were isolated from the left ventricular free wall of rabbit hearts according to Fowler et al. (2018) and from rats according to Bond et al. (2020). Isolations provided myocytes for multiple projects.

2.2 Cell culture and viral transduction

Borosilicate glass coverslips (1 × 5 × 5 mm) were placed in 24-well culture dishes (Thermo-Fisher Scientific, 10380932), pre-coated with laminin (0.5 µg/cm^2; Sigma, L2020) and incubated at 37 ˚C for at least 1 hr. Coverslips were then washed three times with phosphate buffered saline (PBS; Merck, 806552) before acutely isolated cardiac ventricular myocytes (CVMs) suspended in culture medium were added to each well (Figure 4). Cells were plated at a density of 10^4 rod-shaped cells/cm^2, calculated using a haemocytometer. Cells were placed in an incubator (5 % CO_2; 37 ˚C) for 3 hr before culture media was carefully aspirated from each well and replenished with fresh media.

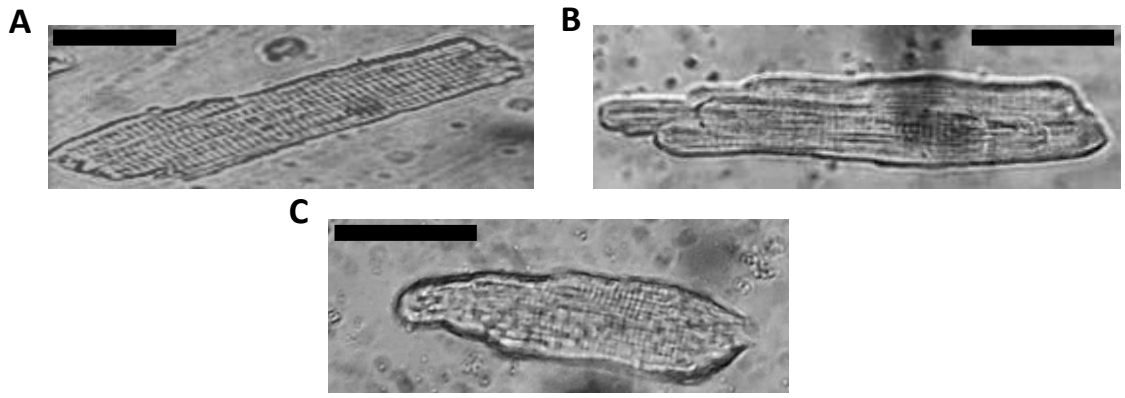

Figure 4. Rabbit ventricular myocytes in short-term culture. Photomicrographs are shown for rabbit ventricular myocytes at days 0 (**A**), 2 (**B**) and 4 (**C**) of culture, as observed under × 40 magnification of a light microscope. Scale bars are 50 µm. The silhouette of a patch pipette is visible in panel B.

For cells being transduced, the fresh media also contained either Ad-GFP (green fluorescent protein; Vector Biolabs, 1060) or Ad-h-JPH2-GFP (Junctophilin-2; Vector Biolabs; Figure 5A) at a multiplicity of infection (MOI) of 50. Virus-free media was used to replace the media bathing cells at day 2 of culture. Culture media was composed of M199 (Sigma, M0650) supplemented with (in mM): L-ascorbic acid (0.1; Merck, A92902), L-carnitine (2; Merck, C0283), creatine monohydrate (5; Acros Organics, 226791000), taurine (5; Merck, T0625), bovine serum albumin (BSA; 0.5 g/l; Merck, A9418) and $NaHCO_3$ (2.2 g/l; Merck, S8761) and penicillin/streptomycin (100X; Merck, 516106). The Vector Biolabs JPH2 protein sequence for the Ad-h-JPH2-GFP used aligned perfectly with the canonical human UniProt JPH2 protein sequence (Q9BR39), and protein sequence alignment between human, rat, and rabbit JPH2 (Figure 5B) shows greater sequence homology between human and rabbit (93.18 %) than human and rat (88.45 %) with highly conserved N-terminal MORN motifs and C-terminal transmembrane anchor regions.

A

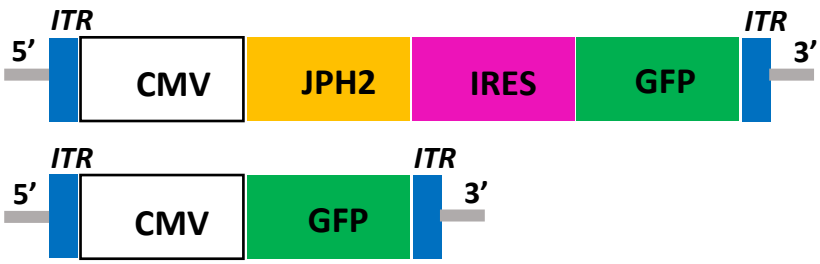

B

```
sp|Q9BR39-1|JPH2_HUMAN      MSGGRFDFDDGGAYCGGWEGGKAHGHGLCTGPKGQGEYSGSWNFGFEVAGVYTWPSGNTF   60
sp|Q9GKY7|JPH2_RABIT       MSGGRFDFDDGGAYCGGWEGGKAHGHGLCTGPKGQGEYSGSWNFGFEVAGVYTWPSGNTF   60
sp|Q2PS20|JPH2_RAT         MSGGRFDFDDGGAYCGGWEGGKAHGHGLCTGPKGQGEYSGSWNFGFEVAGVYTWPSGNTF   60
                           ************************************************************

sp|Q9BR39-1|JPH2_HUMAN      EGYWSQGKRHGLGIETKGRWLYKGEWTHGFKGRYGIRQSSSSGAKYEGTWNNGLQDGYGT  120
sp|Q9GKY7|JPH2_RABIT       EGYWSQGKRHGLGIETKGRWLYKGEWTHGFKGRYGTRQSTSSGAKYEGTWNNGLQDGYGT  120
sp|Q2PS20|JPH2_RAT         EGYWSQGKRHGLGIETKGRWLYKGEWTHGFKGRYGIRQSTNSGAKYEGTWNNGLQDGYGT  120
                           ********************************** ***:.******************

sp|Q9BR39-1|JPH2_HUMAN      ETYADGGTYQGQFTNGMRHGYGVRQSVPYGMAVVVRSPLRTSLSSLRSEHSNGTVAPDSP  180
sp|Q9GKY7|JPH2_RABIT       ETYADGGTYQGQFTNGMRHGYGVRQSVPYGMAVVVRSPLRTSLSSLRSEHSNGTVAPDSP  180
sp|Q2PS20|JPH2_RAT         ETYADGGTYQGQFTNGMRHGYGVRQSVPYGMAVVVRSPLRTSLSSLRSEHSNGTVAPDSP  180
                           ************************************************************

sp|Q9BR39-1|JPH2_HUMAN      ASPASDGPALPSPAIPRGGFALSLLANAEAAARAPKGGGLFQRGALLGKLRRAESRTSVG  240
sp|Q9GKY7|JPH2_RABIT       ASPAADGPALPSPAIPRGGFALSLLANAEA-ARAPKGGGLFPRGALLGKLRRAESRTSVG  239
sp|Q2PS20|JPH2_RAT         ---AADGPTLPLPPVPRGGFALSLLATAEAA----RPPGLFTRGALLGRLRRSESRTSLG  233
                              *:***:** * :***********.***     :  *** ******:***:*****:*

sp|Q9BR39-1|JPH2_HUMAN      SQRSRVSFLKSDLSSGASDAASTASLGEAAEGADE-AAPFEADIDATTTETYMGEWKNDK  299
sp|Q9GKY7|JPH2_RABIT       SQRSRVSFLKSDLSSGASDAASTASLGEGAEGADD-AAPFEADIDATTTETYMGEWKNDK  298
sp|Q2PS20|JPH2_RAT         SQRSRLSFLKSELSSGASDAASTGSLAEGAEGPDDAAAPFDADIDATTTETYMGEWKNDK  293
                           *****:*****:***********.**.*.*** *: ****:******************

sp|Q9BR39-1|JPH2_HUMAN      RSGFGVSERSSGLRYEGEWLDNLRHGYGCTTLPDGHREEGKYRHNVLVKDTKRRMLQLKS  359
sp|Q9GKY7|JPH2_RABIT       RSGFGVSERSSGLRYEGEWLDNLRHGYGCTTLPDGHREEGKYRHNVLVKGTKRRVLPLKS  358
sp|Q2PS20|JPH2_RAT         RSGFGVSERSSGLRYEGEWLDNLRHGYGRTTLPDGHREEGKYRHNVLVKGTKRRVLPLKS  353
                           *************************** ******************.****:* ***

sp|Q9BR39-1|JPH2_HUMAN      NKVRQKVEHSVEGAQRAAAIARQKAEIAASRTSHAKAKAEAAEQAALAANQESNIARTLA  419
sp|Q9GKY7|JPH2_RABIT       NKVRQKVEHSVEGAQRAAAIARQKAEIAVSRTSHARAKAEAAEQAALAANQESNIARSLA  418
sp|Q2PS20|JPH2_RAT         NKVRQKVEHGVEGAQRAAAIARQKAEIAASRTSHAKAKAEAAEQAALAANQESNIARTLA  413
                           *********.******************.******:**********************:**

sp|Q9BR39-1|JPH2_HUMAN      RELAPDFYQPGPEYQKRRLLQEILENSESLLEPPDRGAGAAGLPQPPRESPQLHERETPR  479
sp|Q9GKY7|JPH2_RABIT       RELAPDFYQPGPEYQKRRLLQEILEHSESLLEPPDRG--AAGLPQPPRESPQLHERETPR  476
sp|Q2PS20|JPH2_RAT         KELAPDFYQPGPEYQKRRLLQEILENSESLLEPRERGPG-TGLPERPRESPQLHERETPQ  472
                           :************************:******* :**   :***: ************:

sp|Q9BR39-1|JPH2_HUMAN      PEGGSPSPAGTPPQPKRPRPGVSKDGLLSPGAWNGEPSGE----GSRSVT-PSEGAGRRS  534
sp|Q9GKY7|JPH2_RABIT       PEGGPPSPAGTPPQPKRPRPGASKDGLLGPGAWNGEPSGGSGGEGSRPATPAAAGAGRRS  536
sp|Q2PS20|JPH2_RAT         PEGGPPSPAGTPPQPKRPRPGSSKDGLLSPGAWNGEPGGEGSR-----PATPSDGAGRRS  527
                           **** *************** ******.********.*          :  : ******

sp|Q9BR39-1|JPH2_HUMAN      PARPATERMAIEALQAPPAPSREPEVALYQGYHSYAVRTTPPEPPPFEDQPEPE--VSGS  592
sp|Q9GKY7|JPH2_RABIT       PARPASEHMAIEALQAPPAPSREPEVALYRGYHSYAVRTAPPAPPPFEDDPQPE--AADP  594
sp|Q2PS20|JPH2_RAT         PARPASEHMAIEALQPPPAPSREPEVALYRGYHSYAVRTGPPEPPPLEDEPEPEPEPVPRS  587
                           *****:*:******* *************:********* ** ***:**:*:**  .

sp|Q9BR39-1|JPH2_HUMAN      ESAPSSPATAPLQAPTLRGPE-PARETPAKLEPKPIIPKAEPRAKARKTEARGLTKAGAK  651
sp|Q9GKY7|JPH2_RABIT       DSAPASPATAPGQAPALGNPE-PAPESPAKLEPKPIVPKA----KARKTEARGLSKTGAK  649
sp|Q2PS20|JPH2_RAT         DSEPPSPVSATVQEEESPAPRSRVPAKPATLEPKPIVPKAEPKAKARKTEARGLSKAGAK  647
                           :* * **.:*  *      *.  .  .**.******:***    **********:*:***

sp|Q9BR39-1|JPH2_HUMAN      KKARKEAALAAEAEVEVEEVPNTILICMVILLNIGLAILFVHLLT   696
sp|Q9GKY7|JPH2_RABIT       KKPRKEAAQAAEAEVEVEEVPNTVLICMVILLNIGLAILFVHLLT   694
sp|Q2PS20|JPH2_RAT         KKGRKEVAQEAEAEVEVEEVPNTVLICMVILLNIGLAILFVHLLT   692
                           ** ***.*  *************:**********************
```

Figure 5. Adenoviral constructs. A Graphical representations of adenoviral constructs. Top: Ad-h-JPH2-GFP; cells transduced with this virus are referred to as JPH2+. Bottom: Ad-GFP; cells transduced with this virus are referred to as GFP+. **B** Protein sequence alignment for JPH2. Human (Q9BR39), rabbit (Q9GKY7) and rat (Q2PS20) protein sequences were aligned using the UniProt align tool. The MORN motifs (pink) and the C-terminal transmembrane anchor (blue) are highly conserved. For amino acids in the protein sequences, * = identical, : = conserved, . = similar. CMV = cytomegalovirus promoter. ITR = inverted terminal repeat. IRES = internal ribosome entry site.

2.3 Immunostaining

For fixed cell imaging, cells on glass coverslips were removed from the incubator at day 4 of culture and incubated in Tyrode's solution (see below) containing 1 % wheat germ agglutinin conjugated to Alexa Fluor 680 (WGA; Thermo Fisher Scientific, W32465) for 10 minutes whilst being protected from light. Cells were then fixed in 4 % paraformaldehyde (PFA; Insight Biotechnology, AR1068) for 10 minutes before being washed with PBS three times, and stored at 4 °C in a light-controlled environment, for a maximum of three weeks in PBS with 0.1 % BSA and 0.05 % sodium azide (Fluka Biochimika; 71289). Fixed cells were permeabilised by washing three times with PBS containing 0.1 % Triton-X100 (BDH, 306324N), allowing 5 minutes between washes. Cells were blocked by incubating with 10 % goat serum (NEB, 5425S) in PBS for 30 minutes. Cells were then incubated in PBS containing 0.5 % rabbit polyclonal anti-JPH2 primary antibody (Thermo Fisher Scientific, 40-5300), 2 % goat serum and 2 % BSA for 2 hours. Finally, cells were protected from light and incubated in PBS containing goat polyclonal anti-rabbit IgG secondary antibody conjugated to Alexa-Fluor 568 (0.2 %; Thermo Fisher Scientific, A-11036), 2 % BSA and 2 % goat serum for a further 1 hour before being washed and mounted onto microscope slides using ProLong Gold Antifade (Thermo Fisher Scientific, P36930). Cells were washed three times with PBS between each step post-permeabilization and incubated on a rocking platform.

For cells live-imaged using 3-(4-(2-(6-(Dioctylamino)naphthalen-2-yl)vinyl)pyridin-1-ium-1-yl)propane-1-sulphonate (Di-8-ANEPPS; AAT Bioquest, 157134-53-7), culture media containing 1 % Di-8-ANEPPS was used to replace media at day 4 and cells returned to the incubator for 10 minutes. The cells were then washed with regular media before imaging.

2.4 Imaging and image analysis

Cells were imaged using a Leica SP5 confocal microscope at × 63 magnification (oil-immersion). 1024 × 1024 pixel images were captured sequentially for four line averages at wavelengths of excitation of 488 (Argon), 561 (DPSS) and 633 (HeNe), and wavelengths of emission of 488 (GFP), 568 (JPH2) and 635 (WGA). For each cell, the top and bottom planes in the z-axis were located, and images taken 0.3 microns either side of and including the mid-point.

Image analysis was carried out in Image J (Schneider et al., 2012). Mean staining intensity was calculated by plotting a histogram of pixel intensity (0 - 255) for the region around the middle image of each cell, weighting counts by intensity - with background intensity subtracted. For the analysis of TT regularity (Figure 6), to account for both longitudinal and lateral heterogeneity of staining, fast Fourier transforms (FFTs) were performed for three distinct regions of interest (ROI; one located centrally within the cell and the others at either end of the cell where possible) at each z-depth. FFTs were averaged between the three z-depths for each ROI and three parallel lines drawn perpendicular to the principal axis capturing the peaks of the harmonics. An average profile of these parallel lines was produced for each ROI, plotted in Excel and the Solver function used to calculate a best-fit model according to Equation 1.

Equation 1:

$$y = mx + intcpt + (a.\exp\left(-\frac{(x-b)^2}{2c^2}\right)),$$

where *m* and *intcpt* correspond, respectively, to the slope and intercept of a linear declining baseline, and the equation components in brackets represent a Gaussian component to the spectrum, the parameters being as follows: *a* = amplitude of the first harmonic (F1 peak); *b* = frequency of striations and *c* = standard deviation of the peak. The average amplitude of the first harmonic for the three ROIs was used as a measure of TT regularity (termed 'TT power') for that myocyte.

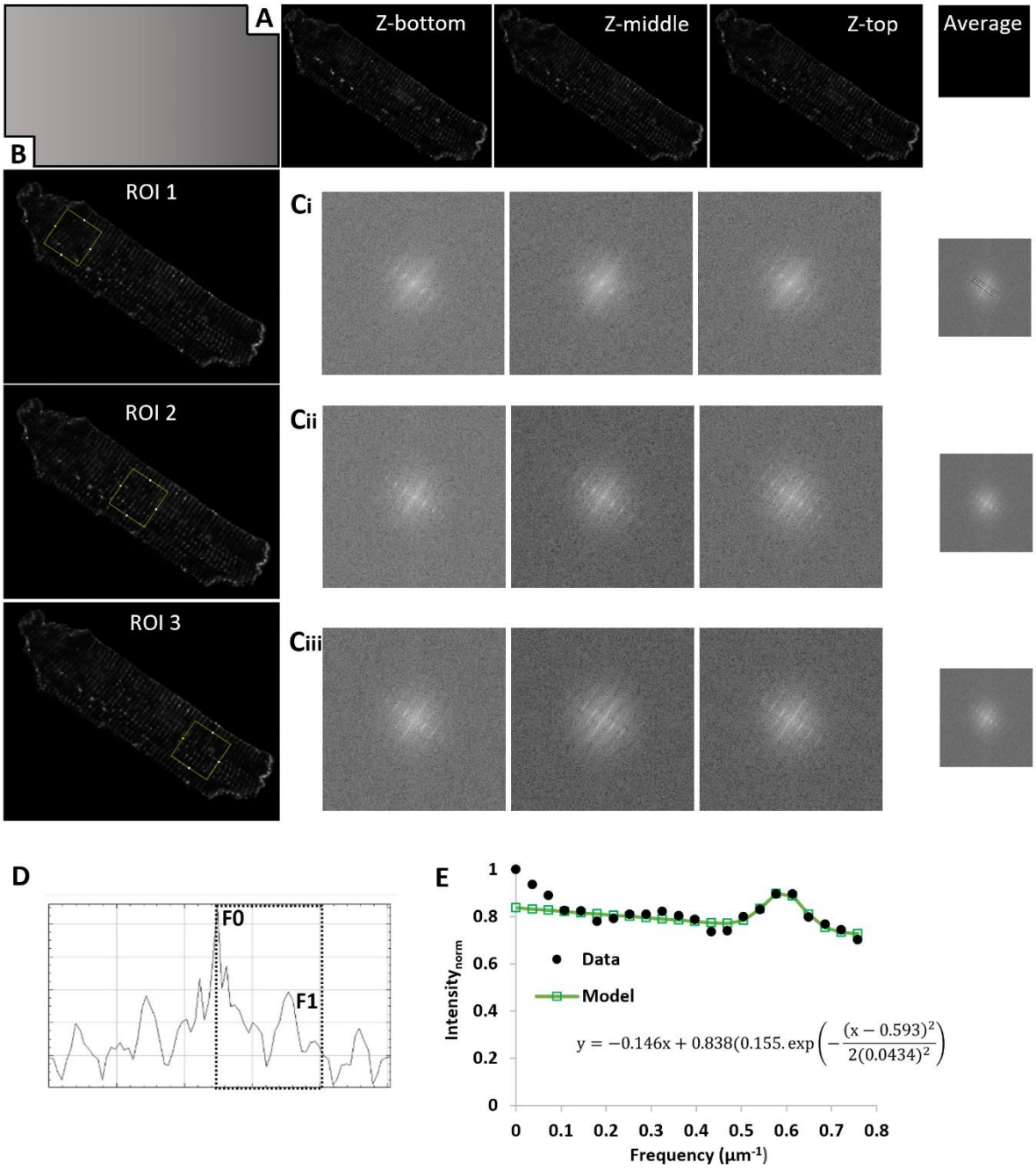

Figure 6. Analysis of T-tubule regularity. A Images of a Day 0 rabbit ventricular myocyte stained with WGA at three z-depths. **B** Images of a Day 0 rabbit ventricular myocyte each showing a region of interest (ROI; yellow squares). The fast Fourier transforms shown in rows **C** correspond to panels A and B, with the FFT average of each row being shown on the right. The FFT average in the first row has three lines drawn perpendicular to the harmonic peaks and Panel **D** shows a plot profile along one of these lines. The selected region capturing the F0 and F1 peaks was exported to Excel and Solver was used to calculate a best-fit model from the average of the three aligned plot profiles (**E**). Aligned plot profiles were analysed in this way to produce models for each ROI, and the mean of *a* in Equation 1 was defined as the TT-power.

2.5 Calcium current (I_{Ca}) recording

Recordings of the whole-cell L-type calcium current (I_{Ca}) were made on the day of isolation (day 0) and at days 1, 2 and 4 in culture. For transduced cells, recordings were taken at day 4 only and cells were selected on the basis of GFP fluorescence. Prior to recording, myocytes were placed in a perfusion chamber mounted on the stage of a CK40 microscope (Olympus) and perfused at 37 ˚C with a Tyrode's solution containing the following (in mM): NaCl 140, KCl 4, $MgCl_2$ 1, Glucose 10, 4-(2-hydroxyethyl)-1-piperazineethanesulphonic acid (HEPES) 5, $CaCl_2$ 2, pH 7.4 (NaOH). Currents were recorded from a holding potential of –80 mV in the whole-cell voltage clamp configuration using an EPC-10 amplifier and Patchmaster software (HEKA GmbH, Germany). The current was subject to two filters in series: Filter 1 was a 6-pole Bessel filter with a corner frequency (f_c) of 10 kHz and Filter 2 was a 4-pole Bessel filter (f_c = 2.8 kHz). The sampling frequency was 50 kHz. Pipettes were pulled from borosilicate glass capillaries (A-M Systems, Washington, USA) using a P-97 pipette puller (Sutter, Novato, CA, USA) and were of 0.7 – 1.4 MΩ resistance when filled with a pipette (intracellular) solution containing (in mM): $CsMeSO_4$ 130, CsCl 20, $MgCl_2$ 2, Mg-ATP 4, Na-GTP 0.2, bis(2-aminophenoxy)ethane tetraacetic acid (BAPTA) 10, HEPES 10, pH 7.2 (CsOH). During recording, the voltage-clamped myocyte was superfused with a potassium-free extracellular solution containing (in mM): NaCl 134, CsCl 4, $MgCl_2$ 1.2, Glucose 11, HEPES 10, $CaCl_2$ 1, pH 7.4 (NaOH) via the perfusion cannula of a rapid-solution switcher (Levi et al., 1996). Current voltage curves were obtained by depolarising the membrane for 200 ms to voltages ranging from -50 to +40 mV for a total of 10 sweeps at 10 s intervals. A pre-pulse (50 ms) to -40 mV was used to inactivate the fast Na^+ current (I_{Na}). I_{Ca} was measured as the difference in current during the test pulse from peak to end-pulse and was plotted against the test pulse potential. The value of the C_{slow} compensation for whole-cell capacitance (in pF) was recorded as an index of membrane surface area. These values were plotted against the numbers of days in culture (see Figure 7) and the data fitted using Equation 2.

Equation 2:

$$capacitance = ((intcpt - c) \times e^{\left(-day/\tau\right)}) + c,$$

where *intcpt* represents the mean capacitance on day 0, *day* is the number of days in culture, τ is a time constant of decay with units of days and *c* represents the time-independent component of whole cell capacitance that does not decline with days in culture.

Current and current density-voltage curves were fitted using a modified Boltzmann equation (Equation 3).

Equation 3:

$$I_{Ca} = \left(\frac{G_{max}\ (X - V_{rev})}{1 + e^{\left((X - V_{half})/k\right)}}\right),$$

where G_{max} is the maximal whole cell conductance, V_{rev} is the effective reversal potential, V_{half} is the half-maximal voltage of activation and *k* is the slope factor for voltage-dependent gating.

A similar protocol was used to examine the time course of the effect of the β-adrenergic agonist, isoprenaline (ISO, 100 nM), on I_{Ca}, with the exception that the membrane was depolarised to +10 mV at each successive sweep. ISO was applied immediately after sweep 5. The interval between sweeps was 10 s. Calculation of ISO-dependent increase of I_{Ca} was achieved by comparing the means of the steady state I_{Ca} under control and post ISO-onset conditions: the first five sweeps were used to calculate the mean for baseline I_{Ca} and the mean of sweeps 12 - 14 for I_{Ca} post ISO-onset.

2.6 Statistics

Data are presented as means ± standard error of the mean (SEM) and 95 % confidence intervals of fit are shown for nonlinear models. Statistical analyses and curve fitting by non-linear regression were conducted using Prism and fitted curves were compared by an extra

sum-of-squares F-test (vs9.5.1, GraphPad Software, Boston, Mass, USA). Statistical tests used are outlined in each figure legend. The limit of statistical confidence was taken to be $p < 0.05$. Sample sizes are reported as n/N, where n is the number of cells and N, the number of animals.

3. Results

3.1 Morphological changes in cultured adult rabbit ventricular myocytes

Adult rabbit ventricular myocytes (ARVMs) maintained in culture exhibit significant morphological changes over time when viewed under a light microscope (Figure 4): a loss of clear striations and cell rounding are evident at day 4 compared with the day of isolation (day 0). Figure 7 shows changes in membrane capacitance, a key index of cell surface area, over four days in culture. Capacitance values were obtained in Patchmaster from the C-Slow correction of the whole-cell membrane capacitance. Membrane capacitance decreased by 26 % over the first day of culture but by only 15 % the following day and a further 21 % over the next two days. An exponential curve was fitted to the data with a time constant of 1.68 days.

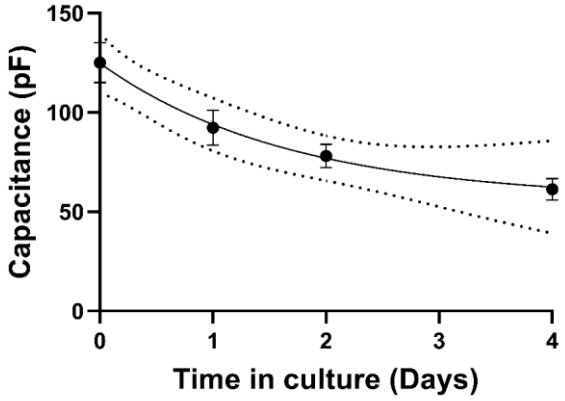

Figure 7. Changes in ARVM capacitance in short-term culture. Membrane capacitance decays exponentially over days in culture with a time constant of 1.68 days. For days 0 – 4: n/N =16/3, 11/3, 18/5 and 6/2. Data points are shown as mean ± SEM, the solid line represents a fit to Equation 2, and the dotted lines show the 95 % confidence intervals of the fit of the model.

WGA conjugated to an Alexa Fluor can be used to stain the sarcolemma (including the TTs) and examples of this are shown in Figure 7A. The staining intensity at day 4 is noticeably less: though the sarcolemma and nuclei remain visible there are no apparent striations. WGA imaging indicated that rabbit ventricular myocytes lose their TTs in short-term culture (Fig. 8A). A fast Fourier transform approach (outlined in Fig. 6) was used to assess TT power - a measure of regularity in TT staining - which was significantly reduced at day 4 of culture,

decreasing approximately threefold from day 0 (Fig. 8B), supporting the suggestion that TTs were lost with days in culture.

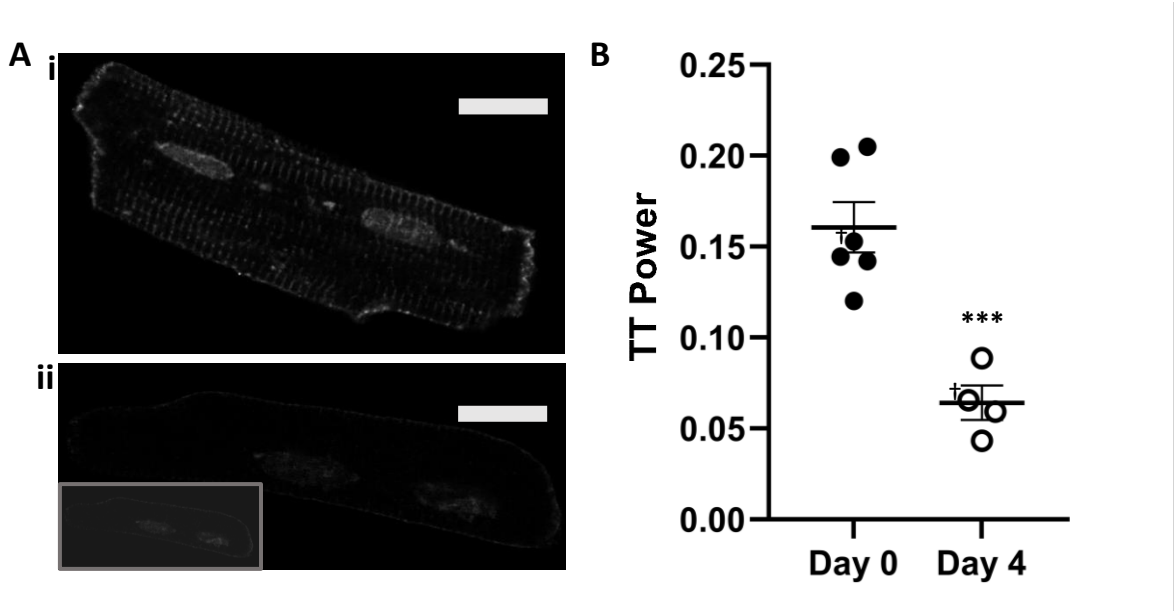

Figure 8. Changes in ARVM T-tubule power in short-term culture. A Representative images of WGA-stained cells at day 0 (**i**) and day 4 (**ii**) of culture. An insert with enhanced contrast is shown in the lower panel. Scale bars are 20 µm. **B** T-tubule power (see Methods 2.4) decreased significantly from day 0 (0.161 ± 0.014; n/N = 4/1) at day 4 (0.064 ± 0.009; n/N = 6/1) of culture (one-tailed unpaired t-test, p = 0.0005). *** p < 0.001; † cell shown in panel A. Data are shown as mean ± SEM with individual values.

3.2 Electrophysiological changes in cultured ARVMs

Using whole cell patch clamp recording, I_{Ca} was examined over four days in culture (Figure 9). Representative traces are shown for days 0, 1, 2 and 4 along with the voltage protocol used and scale bars (Fig. 9A). The I_{Ca}-voltage relations of ARVMs for days 0, 1, 2 and 4 of culture are shown in Figure 9B. Figure 9C shows the same data as current densities normalised to cell membrane capacitance. The I_{Ca}- and I_{Ca} density-voltage relations were well-fitted by a modified Boltzmann equation (Equation 3; solid lines in Figures 9B & 9C). The current-voltage and current density-voltage relations on the days in culture could not be described by a single curve with the same set of parameters ($p < 0.0001$, extra sum-of-squares F-test). Table 1 shows the fitted parameters to both I_{Ca} (upper panels) and I_{Ca} densities (lower panels). Un-normalised G_{max} was significantly reduced in culture compared with acutely isolated (day 0) cells ($p < 0.0001$). G_{max} decreased twofold from 42.1 nS at day 0 to 20.4 nS at day 1 and remained similarly reduced from day 0 at days 2 (18.9 nS) and 4

(20.5 nS) of culture. There was a positive shift of approximately 5 mV in the voltage-dependence of I_{Ca} activation (V_{half}) at day 4 of culture.

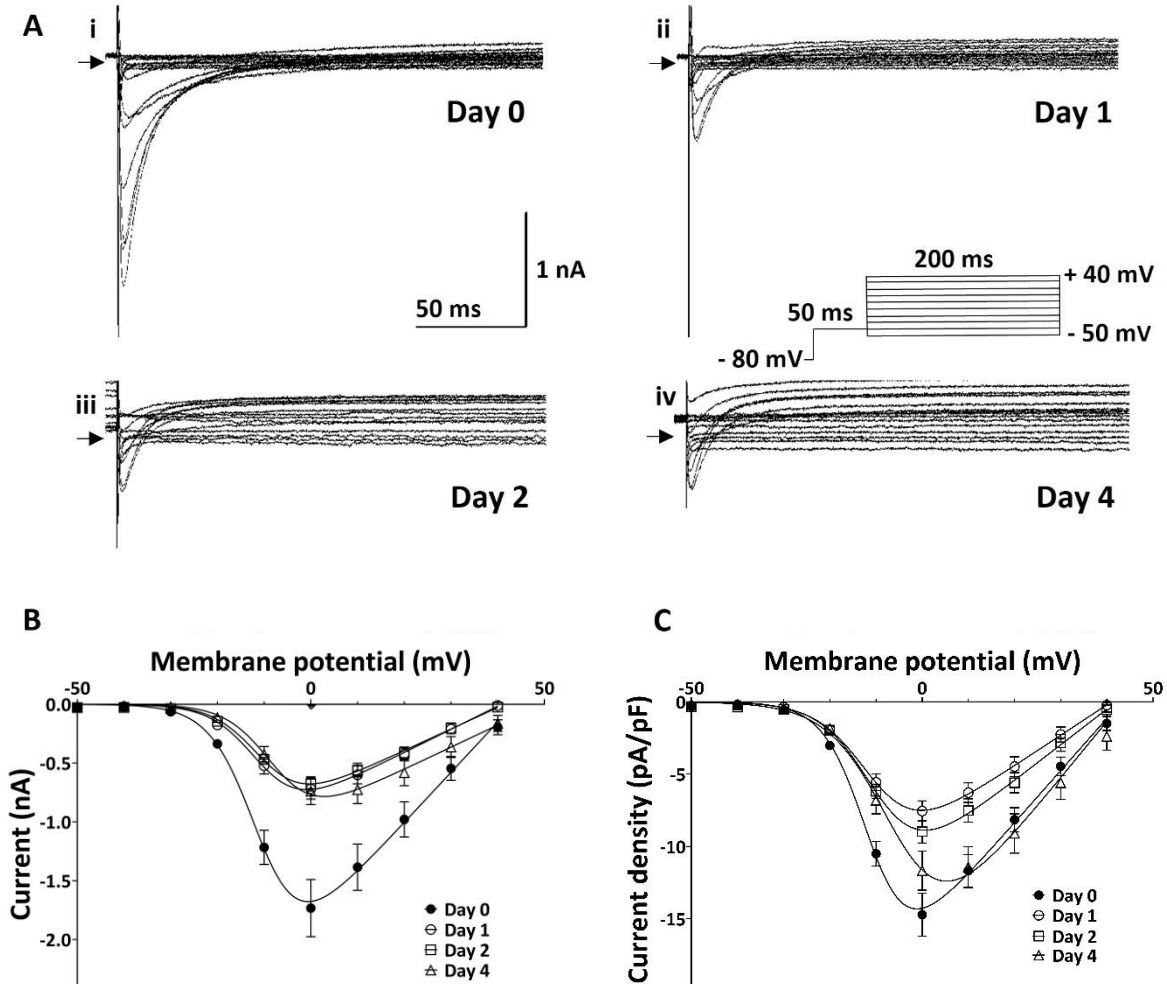

Figure 9. Whole-cell calcium current recordings of cultured ARVMs. A Representative traces of recordings from day 0 (**i**) – 4 (**iv**). The arrows (top left) indicate 0 mV. The 50 ms pre-pulse to - 40 mV is not shown in the traces. **B** Current voltage relation for days 0 – 4 of culture. The curves fitted for days 0 – 4 were significantly different ($p < 0.0001$; extra sum-of-squares F-test). **C** Current density-voltage relation for days 0 – 4 of culture. The fitted curves were significantly different ($p < 0.0001$; extra sum-of-squares F-test). For days 0 – 4: n/N = 11/3, 10/3, 13/5 and 6/2. Data are shown as mean ± SEM. For panels **B** and **C** solid lines represent fits to Equation 3 and fitted parameters are presented in Table 1. I_{Ca} was measured as peak minus end-pulse current.

I_{Ca}	G_{max} (nS)	V_{rev} (mV)	V_{half} (mV)	*k*
Day 0	42.1 (34.4 to 50.7)	43.8 (39.8 to 49.1)	-10.9 (-12.9 to -8.53)	-4.58 (-6.29 to -3.10)
Day 1	20.4 (16.6 to 24.9)	40.5 (37.3 to 44.9)	-10.2 (-12.7 to -7.09)	-5.46 (-7.46 to -3.83)
Day 2	18.9 (15.8 to 22.5)	41.2 (38.2 to 45.0)	-9.70 (-11.8 to -7.07)	-5.37 (-7.12 to -3.86)
Day 4	20.5 (14.2 to 28.7)	48.0 (42.1 to 58.3)	-6.48 (-10.2 to -13.6)	-5.83 (-8.68 to -3.35)
p	< 0.0001	0.474	0.408	0.806
I_{Ca} density	**G_{max} (nS/pF)**	**V_{rev} (mV)**	**V_{half} (mV)**	***k***
Day 0	0.360 (0.312 to 0.413)	43.2 (40.3 to 46.8)	-11.1 (-12.6 to -9.40)	-4.63 (-5.85 to -3.56)
Day 1	0.210 (0.173 to 0.254)	41.0 (37.8 to 45.2)	-10 .4 (-12.8 to -7.54)	-5.52 (-7.39 to -3.99)
Day 2	0.247 (0.206 to 0.294)	42.0 (39.0 to 46.0)	-9.65 (-11.8 to -7.04)	-5.47 (-7.20 to -4.00)
Day 4	0.328 (0.243 to 0.434)	47.4 (42.4 to 55.2)	-6.56 (-9.71 to -2.41)	-5.85 (-8.21 to -3.80)
p	0.0001	0.242	0.0392	0.598

Table 1. Modified Boltzmann curve fitting parameters. Table showing parameters fitted to Equation 3 for data shown in Fig. 9B (upper panels) and Fig. 9C (lower panels); numbers in parentheses are the asymmetric 95 % confidence intervals for each parameter. Fitted parameters were compared by extra sum-of-squares F-test. p values indicate probability that the parameters on each day of culture were drawn from the same population.

The current density-voltage relations showed a similar magnitude reduction in G_{max} at day 1 in culture of 1.7-fold: from 0.360 nS/pF to 0.210 nS/pF; with no overlap in the 95 % confidence intervals (95 % CI). There was also a significant difference between days 0 and 2,

with ~1.5- fold reduction to 0.247 nS/pF and no overlap in the 95 % CI. However, at day 4 of culture, G_{max} was not significantly different from day 0 (0.328 nS/pF).

Whole cell patch clamp was used to investigate the effect of the beta-adrenoceptor agonist, isoprenaline (ISO; 100 nM) on I_{Ca} density across the four days in culture. The normalised I_{Ca} diary plots in Figure 10 show that the ARVMs responded to ISO with an approximate doubling of I_{Ca} on days 0, 1, 2 and 4, with no significant difference in the magnitude of the relative response between days in culture (p = 0.908, W ratio = 0.177, degrees of freedom (DFn) = 3, Welch's one-way ANOVA), suggesting the response to ISO is preserved up to day 4 in cultured ARVMs. Test pulses were applied every 10 s until a post-ISO-onset steady state was reached. Interestingly, the response to ISO seems to be delayed at Day 4. The mean (± SEM) times to half-maximal response ($t_{½}$; in seconds) were as follows for days 0 – 4: 27.5 ± 3.66; 20 ± 0; 33.3 ± 8.82 and 50.0 ± 5.77, respectively. Half-maximal response times were not significantly different (p = 0.0519, F* = 3.82, Brown-Forsythe ANOVA).

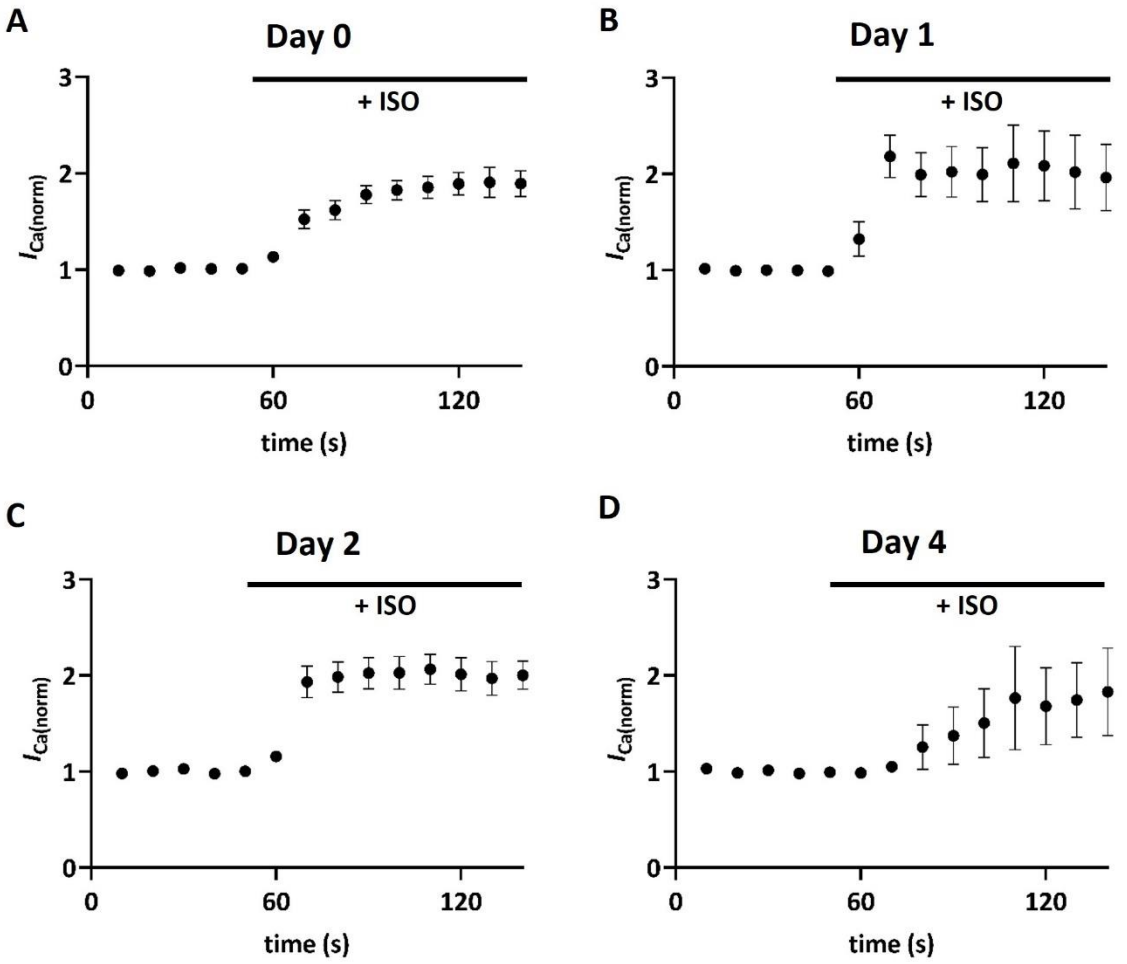

Figure 10. Calcium current during ISO application in ARVMs. Diary plots showing the normalised I_{Ca} response of day 0 (**A**) - 4 (**D**) ARVMs to ISO (100 nM) applied via rapid-solution switcher at test potentials of 10 mV. There was no significant difference between the relative ISO-dependent increase in I_{Ca} ($p = 0.908$, $W = 0.177$, Welch's one-way ANOVA). For days 0 – 4: n/N = 8/3, 6/3, 6/4 and 3/2. Data are shown as mean ± SEM.

Figure 11 shows I_{Ca} density-voltage relationships (left) for days 0, 1, 2 and 4 from paired control and post ISO-onset data. Representative current traces are shown for each day (right). For all days in culture the control and ISO data were best described by different curves (extra sum-of squares F-tests, for each of the four days, $p < 0.0001$). Confidence intervals for the fit of the models are not shown and instead listed in Table 2 for each fitted parameter. G_{max} was increased by ISO by approximately 1.5-fold for each day, however this increase was only significant for days 0 ($p = 0.0076$), 1 ($p = 0.0133$) and 2 ($p = 0.0415$): for day 4 statistical significance was not reached ($p = 0.0826$). These data suggest that the effect

of ISO in augmenting I_{Ca} density is largely preserved in cultured ARVMs, though this can mildly diminish in cells cultured for more than 48 hours. V_{half} seems to be noticeably negatively shifted for all days in culture post ISO-onset (visible as a negative shift in peak current densities in panels A – D). However, this was only significant for days 2, where V_{half} was shifted by -7.2 mV ($p = 0.00191$), and day 4, where V_{half} was shifted by -7.0 mV ($p = 0.0016$); approximately double the magnitude of ISO-induced shift compared to both days 0 and 1. These data suggest that ISO may cause a negative shift in the voltage-dependence of I_{Ca} density, which is profoundly evident in cultured cells at or exceeding two days in culture. Neither V_{rev} nor *k* showed any significant differences between control and ISO across all days in culture.

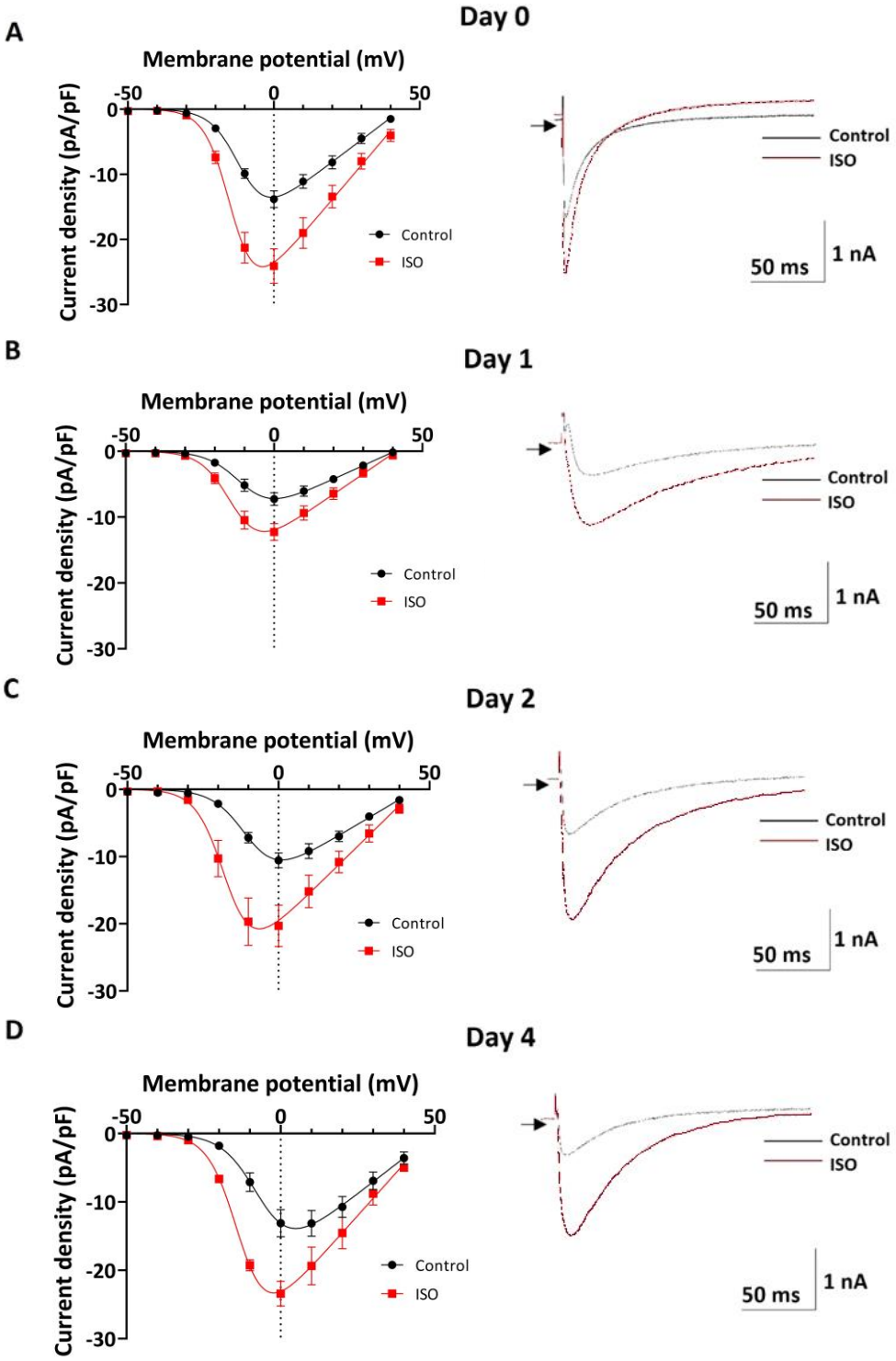

Figure 11. Effect of ISO application on I_{Ca} density in ARVMs in short-term culture. (Left) I_{Ca} density-voltage relationship in the absence & presence of ISO for days 0 (**A**) – 4 (**D**). For days 0 - 4: n/N = 9/3, 6/3, 4/3 and 3/2; black lines/circles = baseline and red lines/squares = ISO; data are shown as mean ± SEM. Solid lines represent fits to Equation 3 and fitted parameters are shown in Table 2. (Right) Representative current traces for given day. Arrows (top left) indicate 0 mV.

I_{Ca} density	G_{max} (nS/pF)	V_{rev} (mV)	V_{half} (mV)	*k*
Day 0 (Control)	0.340 (0.285 to 0.400)	44.0 (40.5 to 48.4)	-10.9 (-12.8 to -8.8)	-4.82 (-6.33 to -3.55)
Day 0 (ISO)	0.528 (0.422 to 0.641)	46.0 (41.5 to 53.2)	-14.2 (-16.5 to -11.8)	-4.24 (-6.01 to -3.11)
p	0.0076	0.553	0.0749	0.721
Day 1 (Control)	0.205 (0.160 to 0.260)	40.7 (36.9 to 46.1)	-10.00 (-13.0 to -6.20)	-5.48 (-7.89 to -3.53)
Day 1 (ISO)	0.309 (0.256 to 0.368)	41.2 (37.7 to 45.8)	-13.5 (-15.8 to -11.1)	-4.98 (-6.64 to -3.68)
p	0.0133	0.868	0.0886	0.723
Day 2 (Control)	0.268 (0.214 to 0.331)	45.7 (41.5 to 51.5)	-9.64 (-12.0 to -6.68)	-5.35 (-7.30 to -3.68)
Day 2 (ISO)	0.470 (0.343 to 0.617)	0.0429 (37.1 to 52.3)	-16.8 (-20.1 to -12.8)	-4.72 (-7.46 to ???)
p	0.0415	0.632	0.0191	0.776
Day 4 (Control)	0.349 (0.239 to 0.492)	50.2 (43.7 to 61.9)	-6.14 (-9.70 to -13.1)	-5.64 (-8.36 to -3.23)
Day 4 (ISO)	0.503 (0.407 to 0.608)	48.9 (44.0 to 55.7)	-13.1 (-15.2 to -10.8)	-4.76 (-6.34 to -3.54)
p	0.0826	0.791	0.0016	0.539

Table 2. Fitted parameters for I_{Ca} density in the absence & presence of ISO. Table showing the parameters and 95 % confidence intervals for fitting of Equation 3 to the I_{Ca} density-voltage curves (represented in Figure 11). For days 0 – 4: n/N = 9/3, 6/3, 4/3 and 3/2; p values indicate probability that fitted parameters were from the same population. ???: indicates that it was not possible to calculate the upper 95 % confidence interval.

3.3 Characteristics of JPH2-transduced ARVMs

Adenoviral constructs (Figure 5A) were used to transduce ARVMs with either green fluorescent protein (GFP) alone, as a control, or JPH2 together with GFP. JPH2-transduced (JPH2+) cells were co-transfected with GFP to distinguish them visually from non-transduced cells on the same coverslip (Figure 12). At day 0 (Figure 12A) there is only autofluorescence evident from a hypercontracted cell. At day 2 - 48 hours post-transduction - there was appreciable fluorescence, with GFP-transduced (GFP+) cells (Figure 12B) appearing brighter than JPH2+ cells (Figure 12C). By day 4, in both GFP+ (Figure 12D) and JPH2+ (Figure 12E) groups, there are some very bright rod-shaped cells, albeit appearing more commonly in the GFP+ group. The fact that the GFP+ cells are, on average, brighter for both days 2 and 4 is likely due to the design of the JPH2+ viral construct because GFP is a secondary gene located downstream of JPH2 (and an IRES element) in a bicistronic vector. The expression of genes located after IRES elements is known to be significantly reduced in comparison to the primary gene (in this case JPH2) (Mizuguchi et al., 2000). The varying background brightness in the righthand column is likely a feature of signal intensity as an auto-exposure setting was used for image capture.

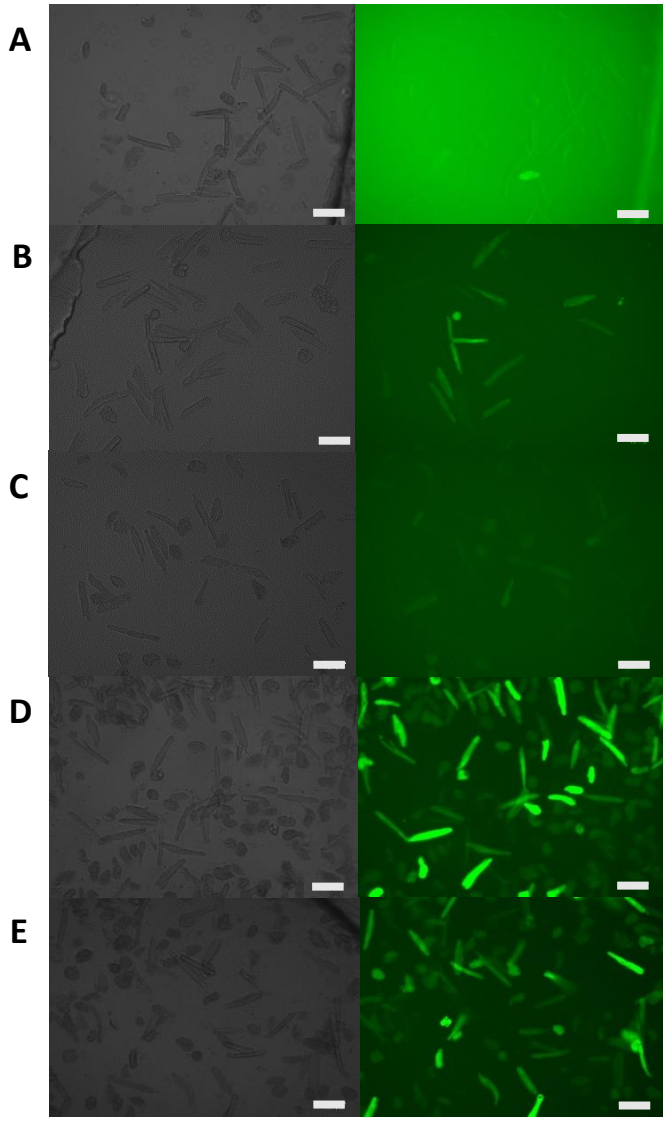

Figure 12. Transduced ARVMs showing green fluorescence on a ZOE fluorescent cell imager. The left column shows brightfield images for day 0 (**A**), day 2 GFP+ (**B**), day 2 JPH2+ (**C**), day 4 GFP+ (**D**) and day 4 JPH2+ (**E**). The right column shows corresponding images using the ZOE green channel (excitation at 480 nm). Scale bars are 100 µm.

Figure 13 shows a quantitative comparison for GFP intensity in day 4 transduced cells which were used for image analysis (the symbols used here correspond to the symbols used subsequently in Figures 16-19). Fluorescence is evident in both populations (though with a wide range) and is greater in GFP+ cells ($p = 0.0135$, one-tailed Mann-Whitney test). It is interesting to note the clustering of data points by animal of isolation in these data. Certainly, for the animal in black in the GFP+ group there is little difference from background suggesting that viral transduction was poor in the cells from this animal available for imaging. In contrast, in the JPH2+ group, the cells from the animal represented by diamonds with dots have much greater GFP intensity than the overall JPH2+ group mean suggesting cells selected from this animal were transduced with more virus or produced more GFP protein (Figure 13).

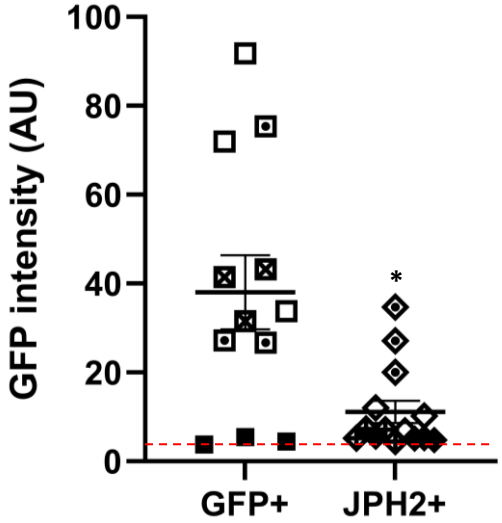

Figure 13. GFP intensity is greater in day 4 GFP+ than in day 4 JPH2+ ARVMs. GFP intensity was significantly less in JPH2+ (11.1 ± 2.53; n/N = 14/4) compared to GFP+ (38.1 ± 8.32; n/N = 12/4) cells (p = 0.0135; one-tailed Mann-Whitney test). * p < 0.05. Data are shown as mean ± SEM with individual values. Symbols denote different rabbit hearts from which myocytes were isolated. Red dashed line indicates background level of fluorescence.

Given that there was a sufficient fluorescent signal being produced to enable the selection of bright cells when patch clamp recording, whole cell I_{Ca} densities were examined in day 4 transduced cells (Figure 14). Some of the data from Figure 9C have been reproduced here (Figure 14A) for convenience and are shown alongside current density-voltage relations for the GFP+ and JPH2+ cells at day 4 in culture (Figure 14B; parameters fitted to Equation 3 shown in Table 3). There was no statistically significant difference between the curves fitted to the data from the GFP+ and JPH2+ cells (p = 0.269, extra sum-of-squares F-test), hence both data are described by one solid line, suggesting that there is no preservation or restoration of I_{Ca} in JPH2+ cells at day 4 in culture.

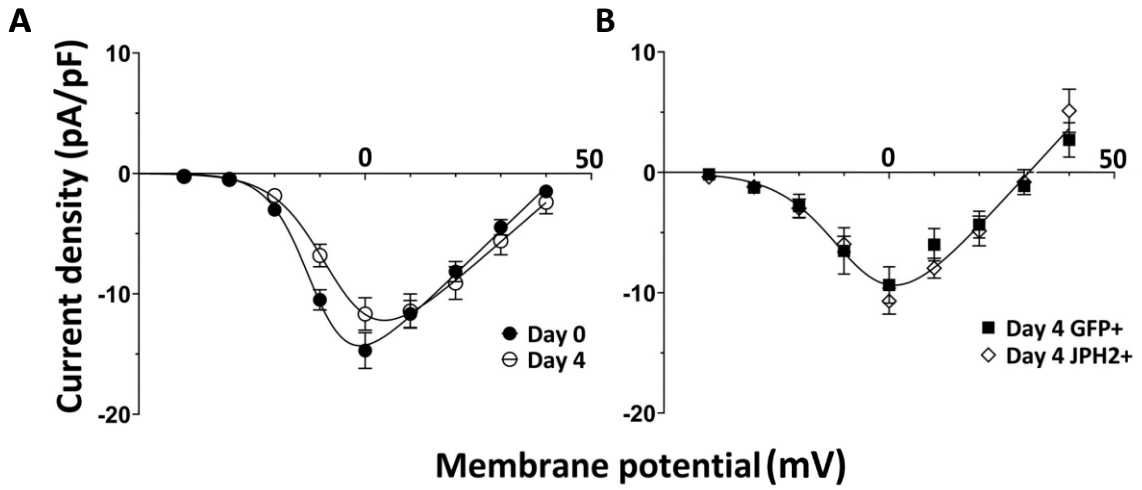

Figure 14. Whole cell calcium current density-voltage relations for non-transduced and transduced ARVMs. A Current density-voltage relation for non-transduced cells from days 0 and 4 of culture (reproduced from Figure 9C) the curves are best described by independent models (p = 0.0002; extra sum-of-squares F-test). Filled circles = day 0, Open circles = day 4. **B** Current density-voltage relations for day 4 GFP+ (n/N = 6/4) and day 4 JPH2+ (n/N = 7/3) ARVMs. Data were fitted to Equation 3. The null hypothesis that a single curve described both data sets was not rejected (p = 0.269; extra sum-of-squares F-test; parameters shown in Table 3). Closed squares = GFP+ and Open diamonds = JPH2+. Data are shown as mean ± SEM.

Current density	G_{max} (nS/pF)	V_{rev} (mV)	V_{half} (mV)	*k*
Day 4 GFP+	0.408 (0.336 to 0.503)	31.0 (29.1 to 33.3)	-7.14 (-10.6 to -2.22)	-6.93 (-9.63 to -4.75)
Day 4 JPH2+				

Table 3. Modified Boltzmann curve fitting parameters. Table showing parameters fitted to Equation 3 for the current density-voltage curves shown in Figure 14B. A single curve described both data sets.

Surprisingly, membrane capacitance at day 4 was 29 % lower in transduced cells than in non-transduced cells (Figure 15), and this was significantly (p = 0.0173, unpaired t-test) different. This result and the spread of data in the transduced cell group suggest that TTs are not preserved in JPH2+ cells. The observed reduction in capacitance in transduced ARVMs may reflect the presence of virus, an effect of viral transduction *per se* or the presence of GFP and is consistent with the idea of leakier/more fragile cell membranes in transduced cells.

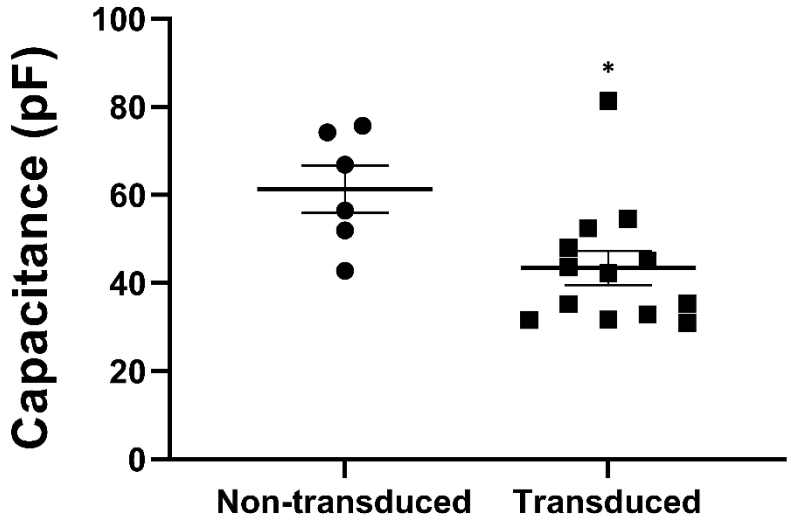

Figure 15. Day 4 membrane capacitance in ARVMs. Day 4 non-transduced cell capacitance (61.3 ± 5.35; n/N = 6/2) was significantly greater (unpaired t-test, t = 2.64, p = 0.0173) than day 4 transduced cell capacitance (43.5 ± 3.88; n/N = 13/4). * $p < 0.05$. Data are shown as mean ± SEM with individual values.

WGA-stained GFP+ and JPH2+ cells were imaged using a confocal microscope and TT staining examined (Figure 16). In both GFP+ and JPH2+ cells, there was an apparent lack of TTs (Fig. 16A). Figure 16B shows TT power in freshly isolated cells and day 4 non-transduced, day 4 GFP+ and day 4 JPH2+ cells. In JPH2+ cells, TT power was only ~50 % of the TT power seen in day 0 ARVMs and this difference was highly significant ($p < 0.0001$, unpaired t-test). Surprisingly, there was no significant difference between GFP+ and JPH2+ cells in terms of TT power. Together, these data suggest that JPH2 transduction does not restore TT power in ARVMs in short-term culture.

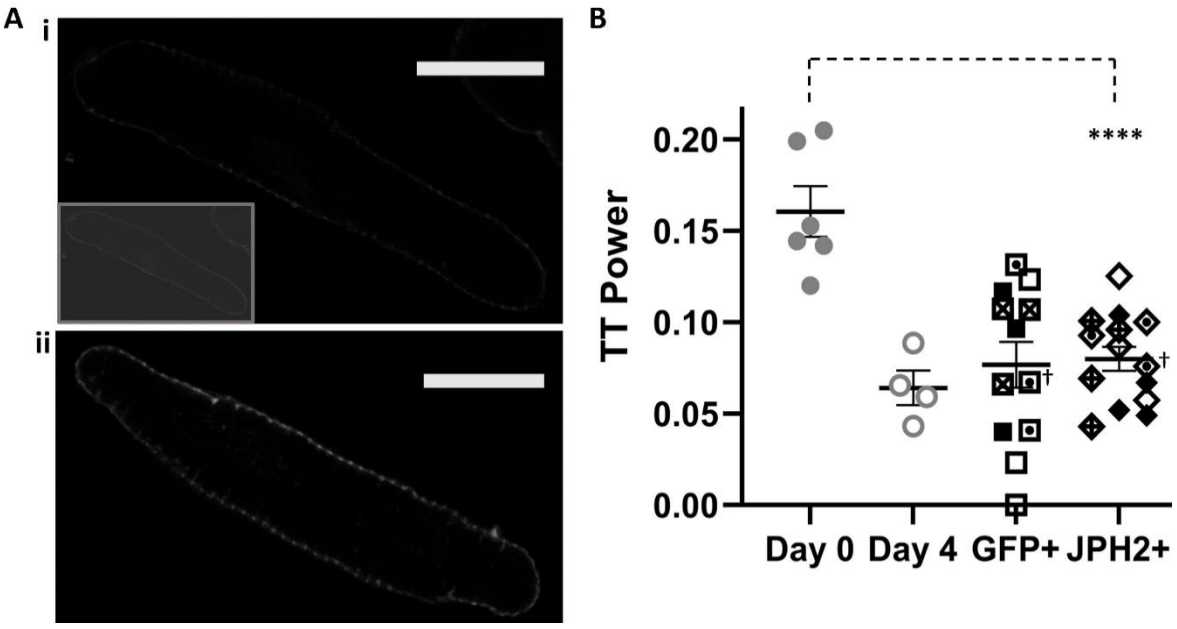

Figure 16. T-tubule power in transduced ARVMs in short-term culture. A Representative images of WGA-stained day 4 GFP+ (**i**) and day 4 JPH2+ (**ii**) cells. An insert with enhanced contrast is shown in the top panel. Scale bars are 20 μm. **B** Analysis of TT regularity in non-transduced (shown previously in Figure 8) and transduced ARVMs. There was no significant difference between GFP+ (0.077 ± 0.012; n/N = 12/4) and JPH2+ (0.080 ± 0.007; n/N = 14/4) cell TT power (unpaired t-test, t = 0.2379, p = 0.814). Day 0 cell TT power (0.161 ± 0.014; n/N = 6/1), was, however, significantly different from day 4 JPH2+ cell TT power (unpaired t-test, t = 6.02, p < 0.0001). **** p < 0.0001; † cell shown in panel A. Data are shown as mean ± SEM with individual values. Symbols in transduced groups denote different rabbit hearts from which myocytes were isolated.

Next, JPH2 antibody staining was examined (Figure 17) and representative images are shown for each group. JPH2 staining intensity was calculated by weighting the total number of pixels within and including the sarcolemma by pixel intensity and then averaging for all intensities, accounting for background intensity. At day 0 (Figure 17A), JPH2 staining was highly regular, taking on a striated appearance – suggesting an abundance of JPH2 at the TTs. High density staining was evident around the nuclei and toward the short edges of the cell. In contrast, staining at day 4 (Figure 17B) was much duller, although a less obvious striated pattern was still apparent. Interestingly, day 4 GFP+ (Figure 17C) and JPH2+ (Figure 17D) cells both show a qualitatively different staining profile in comparison to day 4 non-transduced cells: less regularity, and very apparent bright spots throughout (for a complete Z-depth of day 4 JPH2+ cell GFP, JPH2 and WGA fluorescence/staining, see Supplementary Video).

Quantification of JPH2 staining intensity in ARVMs is shown in panels E (non-transduced) and F (transduced) of Figure 17. The laser power was slightly increased for transduced cells due to difficulty visualising cells when collecting these data. This meant that valid comparisons could not be made between transduced and non-transduced cells and therefore, two distinct sets of axes have been used to present these data. For non-transduced cells (Figure 17E), JPH2 staining reduced significantly, by 30 %, from day 0 to day 4 ($p = 0.0045$). For transduced cells (Figure 17F) JPH2 staining was approximately 20 % lower in GFP+ compared to JPH2+ cells, which was also statistically significant (one-tailed p value = 0.0173).

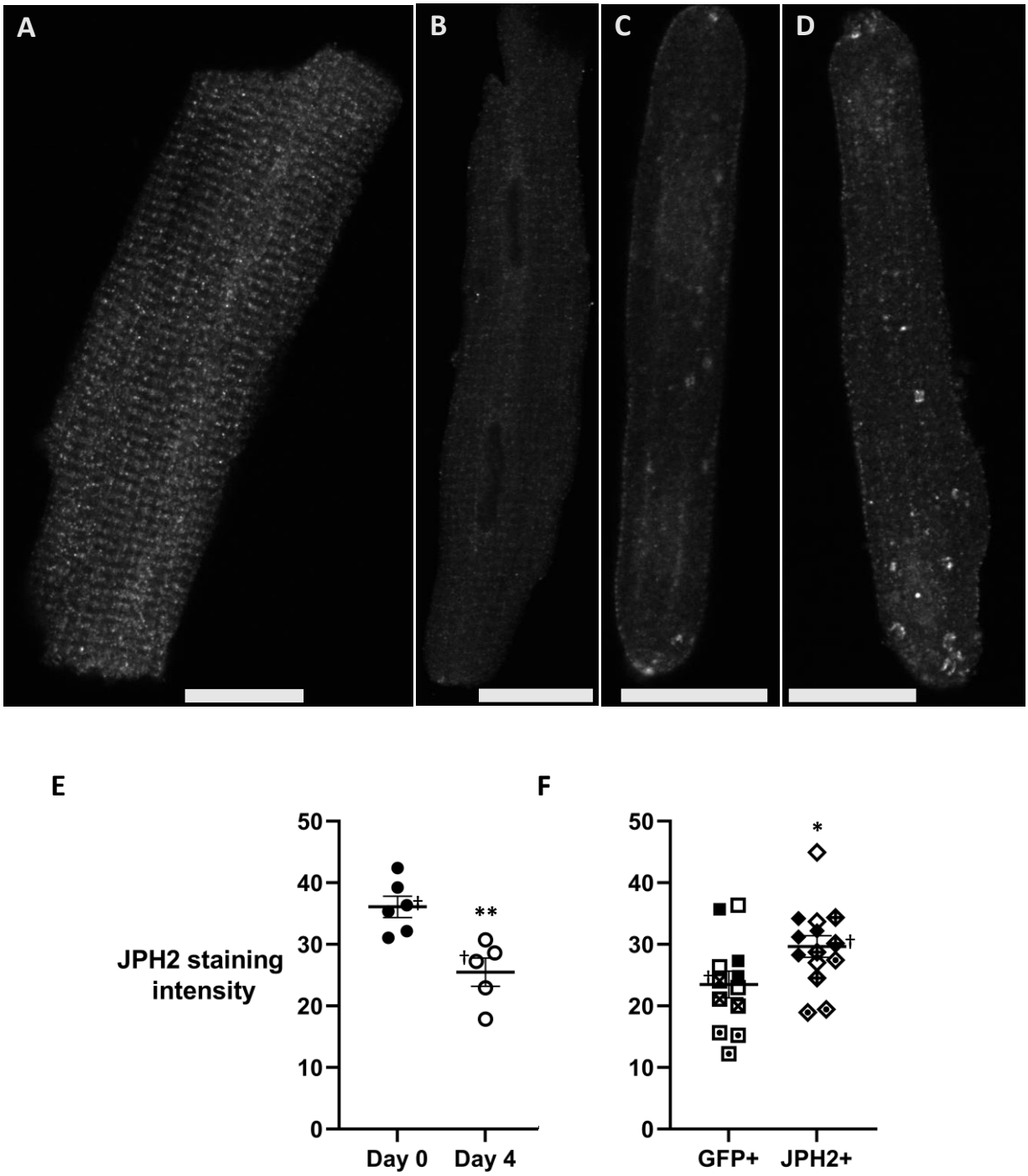

Figure 17. JPH2 antibody staining in ARVMs. Representative images of JPH2 staining for day 0 (**A**), day 4 (**B**), day 4 GFP+ (**C**) and day 4 JPH2+ (**D**). Scale bars are 20 μm. For non-transduced cells (**E**) JPH2 staining intensity (AU) was significantly less at day 4 (25.5 ± 2.29; n/N = 5/1) compared to day 0 (36.1 ± 1.74; n/N = 6/1) of culture ($p = 0.0045$). For transduced cells (**F**) JPH2 staining intensity was significantly greater in JPH2+ (29.7 ± 1.76; n/N = 14/4) compared to GFP+ (23.5 ± 2.16; n/N = 12/4) cells ($p = 0.0173$ (one-tailed)). Standard unpaired t-tests were used to test for significance between group means. * $p < 0.05$, ** $p < 0.01$; † cell shown in panel A. Data are shown as mean ± SEM with individual values. Symbols in transduced groups denote different rabbit hearts from which myocytes were isolated. Two axes are shown because the laser power used to image transduced cells was different.

Figure 18 shows a correlation plot for JPH2 staining intensity and TT power in transduced ARVMs. Neither GFP+ nor JPH2+ groups showed a significant correlation (Pearson's correlation coefficient). This was particularly noteworthy given the large within-group range for both TT power and JPH2 staining intensity in both data sets.

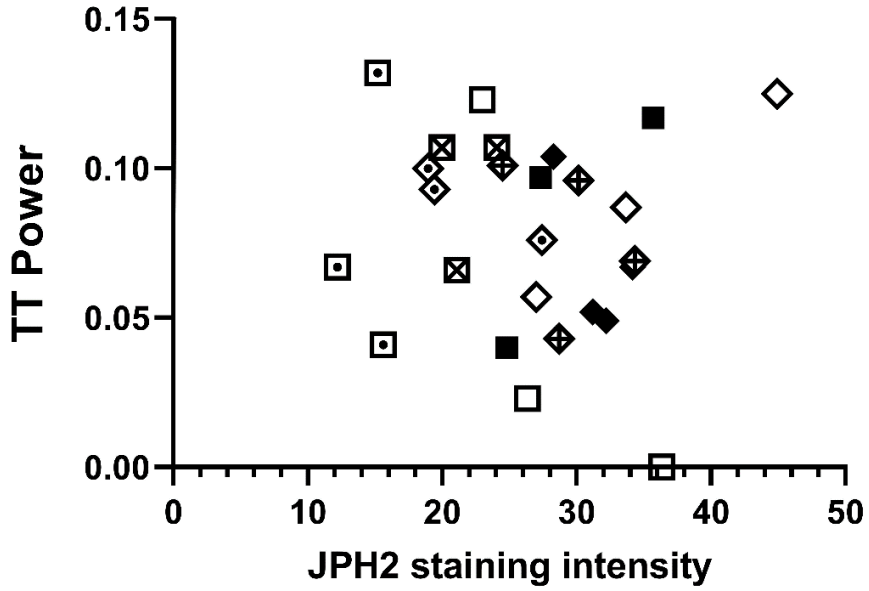

Figure 18. Correlation between JPH2 staining intensity and TT power in transduced ARVMs. There was no significant correlation (Pearson's correlation coefficient) between TT power and JPH2 staining intensity for GFP+ (Squares; R = - 0.217, p = 0.500, n/N = 12/4) nor JPH2+ (Diamonds; R = 0.0515, p = 0.861, n/N = 14/4) ARVMs. Symbols denote different rabbit hearts from which myocytes were isolated.

Figure 19 shows a lack of significant correlation of JPH2 staining with GFP fluorescence intensity in JPH2+ transduced ARVMs (p = 0.522; Spearman's rank correlation coefficient) which is surprising given that it would be expected that the primary transgene in a bicistronic vector would be expressed proportionally to the secondary transgene (Mizuguchi et al., 2000).

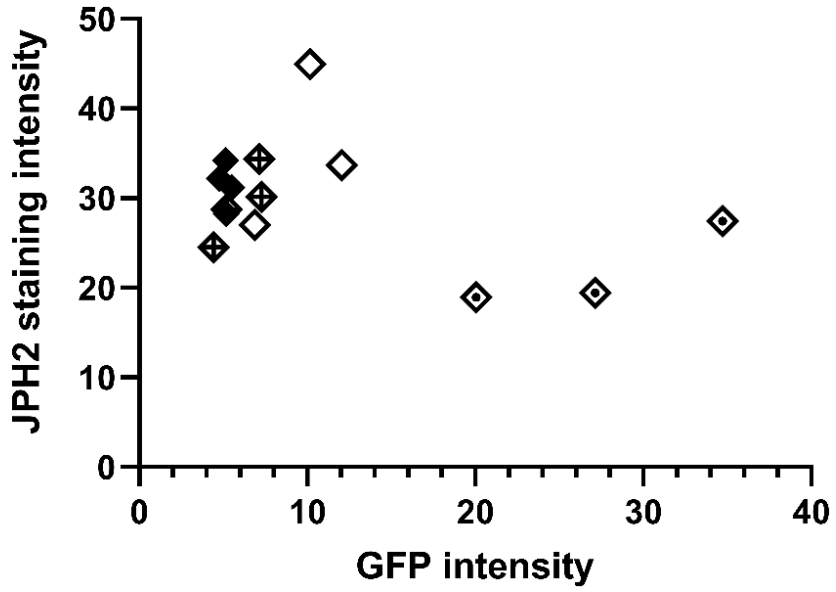

Figure 19. Correlation between GFP intensity and JPH2 staining intensity in JPH2+ ARVMs. There was no significant correlation (Spearman's rank correlation coefficient, S = - 0.187, p = 0.522, n/N = 14/4) between GFP intensity and JPH2 staining intensity for JPH2+ cells. Symbols denote different rabbit hearts from which myocytes were isolated.

3.4 Comparative preliminary data from rat ventricular myocytes

Adult rat ventricular myocytes were cultured and transduced using the same GFP+ and JPH2+ viral constructs, and the same post-isolation methods as used for ARVMs. Representative images of WGA-stained transduced rat cells are shown in Figure 20. Similar to the ARVM data, there was no significant difference in TT power between the GFP+ and JPH2+ transduced rat cells (Figure 20B).

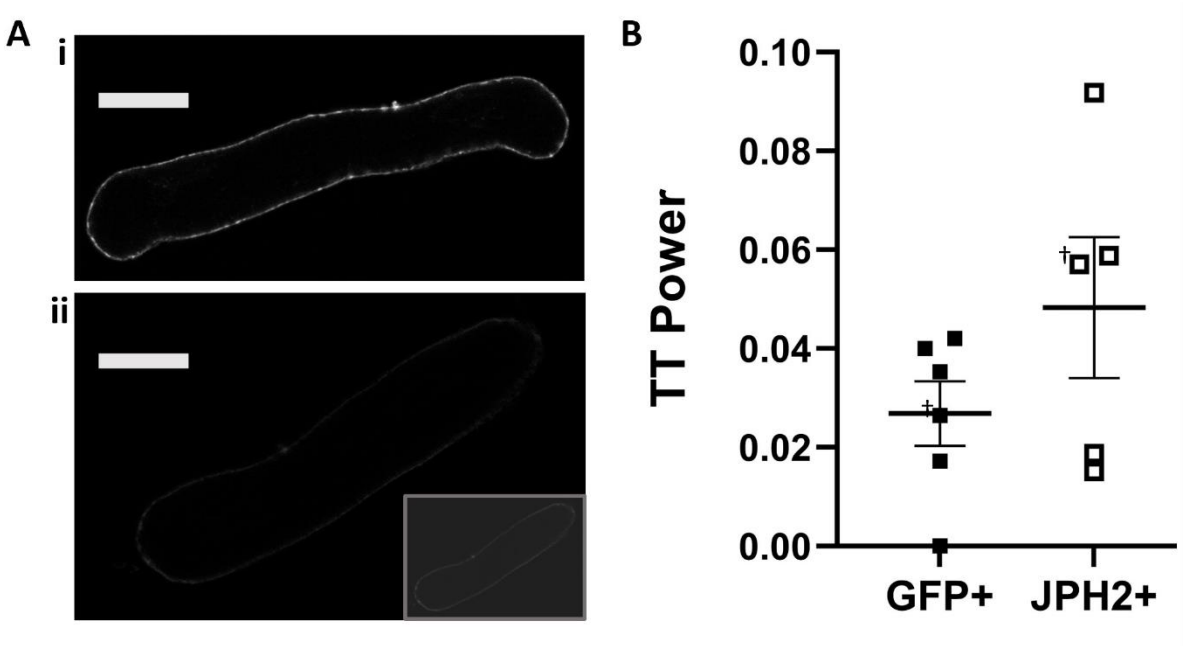

Figure 20. T-tubule power in transduced adult rat VMs. A Representative images of WGA-stained day 4 GFP+ (**i**) and day 4 JPH2+ (**ii**) cells. An insert with enhanced contrast is shown in the bottom panel. Scale bars are 20 µm. **B** TT power was not significantly different between GFP+ (0.268 ± 0.00656; n/N = 6/1) and JPH2+ (0.0483 ± 0.0142; n/N = 5/1) cells (Welch's t-test, T = 1.37, p = 0.166). † cell shown in panel A. Data are shown as mean ± SEM with individual values.

As with ARVMs, JPH2 staining of transduced rat cells (Figure 21) showed a pattern of bright spots throughout the sarcolemma in both groups (Figure 21A), and although the sarcolemmae were noticeably brighter here than in ARVMs – which suggests that JPH2 may be better preserved, more preferentially translated or better translocated to the sarcolemma in rat under these culture conditions - there was no significant difference between JPH2 staining intensity (Fig. 21B) between day 4 GFP+ and JPH2+ transduced adult rat VMs.

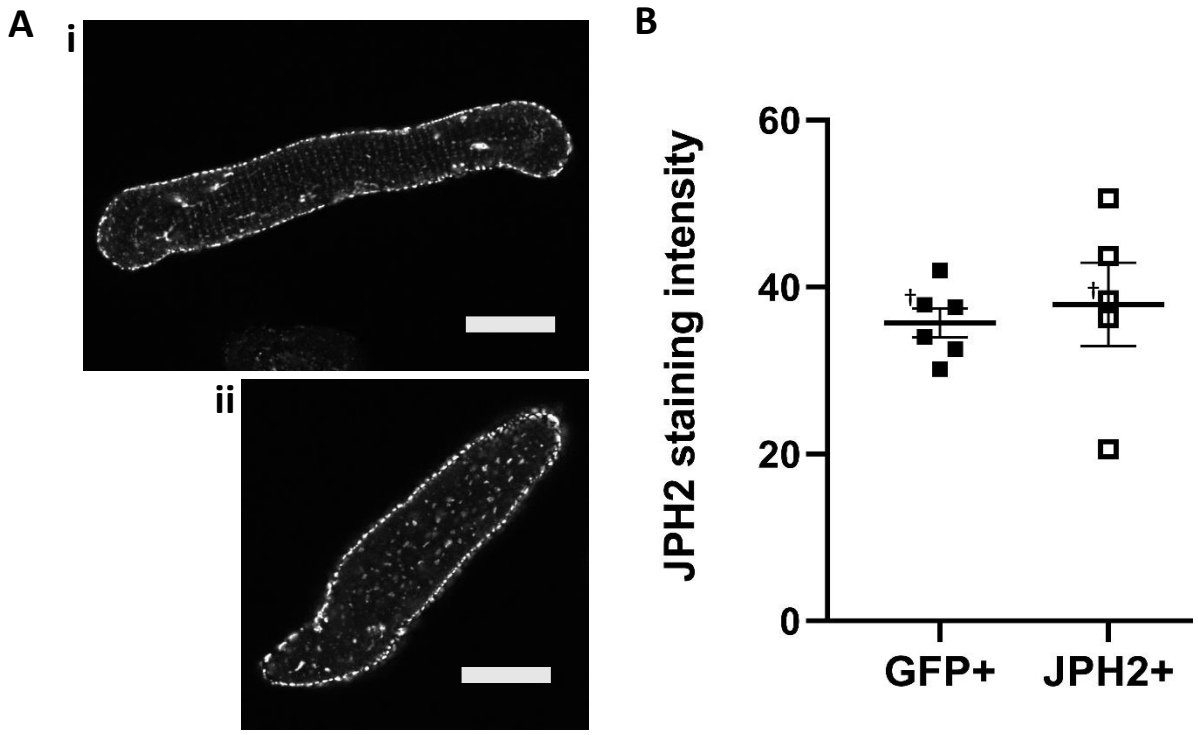

Figure 21. JPH2 antibody staining in transduced adult rat VMs. A Representative images of JPH2 staining for day 4 GFP+ (**i**) and day 4 JPH2+ (**ii**). Scale bars are 20 µm. **B** JPH2 staining intensity was not significantly different between GFP+ (35.7 ± 1.74; n/N = 6/1) and JPH2+ (37.9 ± 4.99; n/N = 5/1) cells (Welch's t-test, T = 0.420, p = 0.692). † cell shown in panel A. Data are shown as mean ± SEM with individual values.

A correlation analysis was performed for GFP intensity and JPH2 staining intensity (Figure 22), which showed no significant correlation between GFP intensity and JPH2 staining intensity.

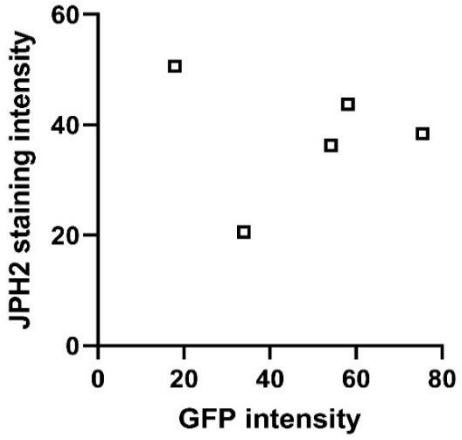

Figure 22. Correlation between GFP intensity and JPH2 staining intensity in JPH2+ adult rat VMs. There was no significant correlation (Spearman's rank correlation coefficient, S = - 0.100, p = 0.950, n/N = 5/1) between GFP intensity and JPH2 staining intensity for JPH2+ cells.

4 Discussion

4.1 Structural changes occur over time in culture in ARVMs

The data presented in Figure 7 show that ARVM membrane capacitance decreases exponentially with time in culture with a time constant of 1.68 days. The loss of membrane capacitance over days in culture likely corresponds to a loss of TTs, an idea that is closely supported by the imaging data and loss of TT power in Figure 8. Loss of TTs during short-term culture is a feature observed in other studies of cultured adult ventricular myocytes (VMs) (Mitcheson et al., 1996, Pavlovic et al., 2010). Interestingly, mouse VMs do not seem to suffer a significant loss of TTs or membrane capacitance over a similar number of days in culture (Pavlovic et al., 2010), though TT derangement can be seen in mouse models of HF (Reynolds et al., 2016). The molecular dynamics of TT disruption and loss through either cell culture or HF are not fully clear, although the overexpression of the membrane scaffolding protein JPH2 has been suggested to preserve TT regularity and density in both conditions (Gross et al., 2021, Poulet et al., 2021, Reynolds et al., 2016). In this study, the hypothesis that JPH2 overexpression protects against TT loss and restores I_{Ca} density in ARVMs in short-term culture was tested. Whilst the lack of change in I_{Ca} density and TT power in JPH2+ cells in comparison to GFP+ cells seemed to suggest that the hypothesis should be rejected, the unexpectedly low level of JPH2 overexpression and the irregular JPH2 staining intensity profiles of transduced ARVMs in comparison to non-transduced ARVMs provide cause for caution in dismissing a role for JPH2 in the maintenance of the TT network.

4.2 I_{Ca} continues to decrease with days in culture but I_{Ca} density partially recovers

Figure 9 and Table 1 show that the G_{max} for I_{Ca} decreased approximately twofold in cultured ARVMs compared to acutely isolated ARVMs. This change in G_{max} and a commensurate loss in I_{Ca} were evident even at 24 hours in culture, whereas significant ARVM whole-cell capacitance remained at this time point (92 pF), having only decreased by a quarter of day 0 whole-cell capacitance, presumably indicating that the loss of TTs in culture occurred more slowly than the reduction in I_{Ca} and I_{Ca} density (see Figure 7). Supporting this view, Mitcheson and colleagues showed in AVRMs loaded with the lipophilic dye, di-4-ANEPPS that significant TT membrane staining remained after one day in culture (Mitcheson et al.,

1996). Taken together, these findings suggest that the loss of I_{Ca} over the first 24 hr in culture may not solely be accounted for by the loss of TT membrane. However, studies using random access multiphoton microscopy have suggested that regions of the TT network that remain connected to the cell exterior following disruption by osmotic shock or HF can become electrically uncoupled from the surface membrane (Crocini et al., 2016, Sacconi et al., 2012). If such electrical isolation occurred in the cultured cells in this study, then LTCCs in such regions may not have contributed to whole cell I_{Ca}. Having said this, the evidence for 'electrical uncoupling' comes from fluorometric recordings using a voltage-sensitive membrane probe (di-4-AN(F)EPPTEA) and it is not clear whether LTCC would be electrically isolated under voltage-clamp conditions (Sacconi et al., 2012). In any case, given that there was no further reduction in G_{max} at days 2 and 4 of culture, it would seem therefore that loss of I_{Ca} in short-term culture involves processes in addition to the uncoupling of TT from the sarcolemma. Interestingly, when one considers I_{Ca} density – which accounts for changes in membrane capacitance during cell culture - then the absence of a significant difference between day 0 and day 4 I_{Ca} density for G_{max} suggests that LTCC availability is in fact partially restored, despite the loss of TTs. The fitted G_{max} is slightly greater at day 2 than at day 1, suggesting that the processes underlying this restoration begin between day 1 and day 2.

The gradual recovery of I_{Ca} density could be explained by the following: Firstly, an electrical uncoupling of LTCCs from the surface membrane occurs relatively early due to the TT 'remodelling' process of ARVMs in culture. Secondly, that there is a delay associated with the LTCC insertion into the sarcolemma, perhaps from de novo transcription and trafficking and/or from recycling and membrane reinsertion. It has been suggested that JPH2 coupled to the SR remains in complex with LTCCs despite TT loss (Poulet et al., 2021), and perhaps these interactions are broken over a longer time period such that the pool of LTCCs free to be trafficked to the sarcolemma increases – which would help explain the gradual restoration of I_{Ca} density at day 4. Nexilin, another structural protein which spans the dyadic cleft; interacting with both TTs and the SR (Liu et al., 2019) might also be involved in this complex. Given that the close juxtaposition of LTCC to RyRs at the dyad is required to ensure efficiency of ECC (Cannell and Kong, 2012), such inherent structural stability of calcium release unit microdomains might seem an evolutionarily sound property. In terms of LTCC transcription and trafficking/recycling, the delay in I_{Ca} recovery could be exacerbated by

strenuous demand on cellular resources due to the scale of changes occurring in culture, i.e. as the cell 'remodels' and TTs are lost. Interestingly, it has been shown in failing VMs that LTCCs are redistributed to the sarcolemma and show a calmodulin-dependent kinase II-dependent increase in open probability (Sanchez-Alonso et al., 2016) and perhaps such a change in LTCC open probability also contributes in the observed recovery of I_{Ca} density here. Additional microscopic changes occurring over time in culture could also contribute to the observed loss/recovery of I_{Ca} density. For example, via changes in Cav3-dependent PKA regulation of LTCCs (Bryant et al., 2018).

Another interesting feature of day 4 ARVMs is that the fitted V_{half} is approximately 5 mV more positive than for days 0 – 2. It seems evident from the plotted graph (Fig. 9C) however that there is no change in voltage-dependence of activation at day 4. As this change is observed for day 4 and not days 1 and 2, a potential, and simple, explanation would be that it pertains to changes in cell metabolism arising from time in culture. It could relate also to the reinsertion of LTCCs into the sarcolemma, but not simply their loss from TTs: the reinserted channels could be missing something from their local environment that modulates gain or voltage, although this seems to be contrary to the previously suggested idea of increased channel open probability at day 4 in culture contributing to the recovery of I_{Ca} density.

4.3 The response of ARVMs to ISO is preserved over days in culture

The mean $t_{½}$ for the increase in I_{Ca} in response to ISO (Fig. 10) was longer at day 4; although this was not statistically significant, perhaps partly due to the small sample size, but also because of the long intervals between pulses (10 s) giving limited time resolution. If day 4 $t_{½}$ was indeed longer then this could be the result of reduced availability of second messengers of the β-adrenergic signalling pathway (Liu et al., 2020) in culture; altered cell metabolism associated with time in culture or even of diffusional limitation of ISO to beta-adrenoceptors as the sarcolemma becomes creased with a loss of cell volume and cell rounding (Mitcheson et al., 1996).

The data in Table 2 suggest that the relative ISO-dependent augmentation of I_{Ca} is largely maintained in cultured ARVMs, a finding which has been observed previously in adult guinea pig VMs (Pabbathi et al., 2002). Given that beta-1 adrenoceptors are the predominant

isoform in VMs (Lohse et al., 2003) and that beta-2 adrenoceptors, which are exclusively found at the TTs (Bathe-Peters et al., 2021) also couple to G_i (which reduces adenylyl cyclase activity, cAMP synthesis and PKA-dependent phosphorylation of LTCCs) (Woo and Xiao, 2012), it may be unsurprising that this augmentation is preserved in response to a potent stimulus (100 nM ISO), even when TTs are lost in culture. It is interesting to note however, that ISO-dependent augmentation of I_{Ca} in detubulated rat VMs has been shown to be reduced by half compared to control cells (Brette et al., 2004a). Whilst the authors suggested that this is indicative of beta adrenoceptor signalling in TTs being better coupled to t-tubular $I_{Ca,}$ an idea consistent with more recent data on TT microdomains (Wright et al., 2018), it could also be that the detubulation process negatively impacts the ability of beta-1 stimulation to promote sarcolemmal I_{Ca} in a manner not observed in VMs where TTs have been lost due to time in culture. However, in failing human VMs ISO-dependent augmentation of I_{Ca} is also not preserved (Chen et al., 2002). Overall, then, these data suggest that cell culture-associated loss of TTs is not a good model for studying adrenergic signalling in HF.

The I_{Ca} density-V relations for each day in culture showed a negative shift in the presence of ISO, which was statistically significant for both days 2 and 4 (Table 2). These data, specifically that the negative shift in V_{half} appears to be more pronounced as time in culture increases up to day 4, appears to be at odds with a report from human VMs where HF VMs were not found to show this negative shift, whereas healthy VMs did (Chen et al., 2002). This provides further support to the suggestion that the short-term cultured-cell phenotype is not a good parallel of the HF phenotype in terms of adrenergic responsivity of LTCCs, though it is worth noting that failing cells used by Chen et al. (2002) were of variable aetiology. Reports from acutely isolated rat VMs indicate that 1 µM ISO produced a more profound (-10 mV) shift in peak I_{Ca} (Tiaho et al., 1991), in comparison to the -3 mV shift observed here in acutely isolated ARVMs, albeit with a 10-fold increased dose; however experiments in guinea pig did not observe any such voltage shift over a range of ISO concentrations up to and including 1 µM (Kameyama et al., 1985). It is difficult to draw conclusions from the paired data in Figures 10 and 11 as the sample sizes involved were small, especially for later days in culture where the observed shift in V_{half} was most notable.

It is interesting to note in the representative traces that the rate of decline appears much more rapid at day 0 and this may represent loss of LTCC-RyR coupling at TTs, meaning smaller global transients and hence retarded calcium-dependent inactivation of LTCC. However, Brette et al., (2004b) showed that the effect of loss of TTs through detubulation is dwarfed by the effect of including 10 mM of the calcium buffer BAPTA in the internal pipette solution.

4.5 GFP+ and JPH2+ ARVMs have similar I_{Ca} and TT power at day 4 of culture

Having successfully established and characterised ARVMs in culture, it was next necessary to establish successful viral transduction. Using a bicistronic vector with JPH2 as the primary transgene and GFP under an IRES was, in principle, an efficient way of achieving this. A pilot was done for a range of MOIs – between 10 and 200 – and showed no appreciable benefit in terms of increased percentage of fluorescent cells with increased MOI within this range (data not shown). An MOI of 50 was chosen to be used for the study based on these data and data from other studies using adenoviral vectors in VMs (Zhou et al., 2000). The images in Figure 12 strongly suggest that some of the ARVMs shown are expressing significant levels of GFP at day 4 in culture, indicating successful viral transduction, mRNA transcription and translation of GFP. There are clearly cells that are present in the lefthand column of Fig. 12 panels D and E that are not visible at all in the corresponding right hand column which also suggests that background fluorescence is very low/negligible in rod-shaped cells. The lack of background fluorescence for days 0 and 2 in Figure 12 is consistent with this idea. It is therefore possible that the GFP intensity 'background' line in Figure 13 is overly conservative and does not in fact represent autofluorescence. These points are worth consideration as for one animal in the GFP+ group, and more generally in the JPH2+ group, GFP intensity is not much greater than 'background' signal intensity. Overall, there is clear evidence of at least some successful transduction of the cells used for image analysis and as expected, GFP intensity was significantly greater in GFP+ cells where the GFP transgene was not under an IRES.

Using GFP fluorescence as a marker of successful transduction, selection of transduced ARVMs using fluorescence microscopy for measurement of I_{Ca} using patch clamp electrophysiology was straightforward and guaranteed that only bright cells could be

selected (as only they were visible). Surprisingly, the data showed no significant difference between GFP+ and JPH2+ cells in terms of current density-V relation. The single curve that described both data sets was also not dissimilar from day 4 non-transduced cells in terms of peak current density (cf, Fig. 14B with Fig. 14A), though these cells showed no shift in V_{half} relative to the I_{Ca} density-V relation at day 0. This could imply that the observed shift in V_{half} in non-transduced ARVMs is attributable to random variation in the data rather than a result of time in culture. It was also the case that transduced cells seemed to show a greater leak current towards the end of recording, perhaps resulting from increased membrane fragility due to the presence of the virus, of GFP, or arising from the transduction process. In addition, transduced cell membrane capacitance was less than in non-transduced cells, and one could imagine a smaller surface area would be more susceptible over time to damage arising from patch pipette seal formation. These data suggested that JPH2 overexpression had no appreciable effect in preserving or restoring LTCC number or open probability in ARVMs at day 4 of culture.

Given that there was no significant difference in I_{Ca} density between transduced cells, it seemed unlikely that JPH2+ cells would have better preserved TTs in comparison to GFP+ cells, a view that was validated by membrane capacitance and TT power data. The lipophilic dye, Di-8-ANEPPS was also used to test whether the lack of TT staining might be attributable to a dye-dependent effect of WGA, which instead of being lipophilic binds to membrane glycoproteins (Fodero et al., 2001). Observing both qualitatively and quantitatively (TT power; not shown for Di-8-ANEPPS) similar results for both dyes argue against this notion.

Although the data from this study show that TTs are still absent at day 4 in JPH2+ cells, it is worth discussing possible reasons as to why the range for TT power might be so large – though the fact that this is true for both GFP+ and JPH2+ cells suggest it was likely not due to variability in JPH2 expression, assuming that JPH2 expression was indeed significantly greater in JPH2+ cells. There is no major clustering of data points either side of the mean based on animal of isolation, suggesting isolation-dependent variability was also not a major factor. It seems more likely that inherent heterogeneity in ARVM ultrastructure and how individual cells responded to four days in culture may be the source of this variability. It is also feasible that variability in the data arises in part due to limitations of the analysis used, i.e., the FFT being two and not three dimensional.

4.6 JPH2 staining is greater in JPH2+ compared to GFP+ ARVMs but JPH2 staining does not correlate with TT power or GFP intensity

A major advantage of using WGA to stain ARVMs was that it enabled coimmunostaining with anti-JPH2 antibodies. As expected, JPH2 staining intensity was significantly greater in JPH2+ cells compared to GFP+ cells - but only by 26 % on average. In stark contrast, the study by Poulet et al. (2021) observed an approximately 300 % increase in JPH2 staining at day 4 in JPH2+ adult rat VMs in comparison to control (Poulet et al., 2021). As seen in the TT power data, the spread of JPH2 staining intensity data was very wide, yet there was no correlation between JPH2 staining intensity and TT power, suggesting either that the level of JPH2 expression was too low to elicit a physiological effect, or that ARVMs are different to adult rat VMs in terms of JPH2-dependent rescue of TTs in culture. It is worth mentioning that Poulet et al. (2021), using Western blot, observed sixteen times less JPH2 at day 4 compared to day 0 in culture in non-transfected cells, whereas the immunostaining analysis here showed only a 30 % reduction in JPH2 staining. Given the time and resources, it would have been valuable to carry out a Western blot to better quantify the level of JPH2 expression in this study in terms of both days in culture and between transduced ARVMs.

Strangely, there was also no correlation between GFP intensity and JPH2 staining intensity suggesting that cells fluorescing more brightly did not equate to those cells expressing more JPH2, as might have been assumed. Whilst GFP still served as a marker of transduction, this finding raises the question as to whether there was a problem with the viral vector sequence or coding sequence for JPH2 that limited JPH2 translation or expression. The apparition of bright spots of JPH2 staining in transduced cells is also odd as it could be interpreted that these (presumably) dense regions of JPH2 protein - that were absent in non-transduced cells (Figure 17) - must be produced from exogenous JPH2 gene. However, it could also be that the virus or transduction process interferes with the endogenous JPH2 expression profile of ARVMs at day 4 in culture. The idea that the presence of GFP was a causal agent of any defect in JPH2 expression seems unlikely as one would expect a negative correlation between GFP intensity and JPH2 staining intensity, which was not the case. It also seems unlikely that there was a problem with the JPH2 transgene or viral vector as the construct used was very similar to the one used by Poulet et al. (2021), although with the addition of the IRES element/GFP tag and no human influenza hemagglutinin (HA) tag.

Therefore, to further investigate this critical issue and test that there was no species difference in the expression of the exogenous JPH2 from the viral vector, it seemed prudent to carry out the experiment using adult rat VMs.

4.7 Results of transduction with GFP+ and JPH2+ virus are similar in rat and rabbit VMs

Transduced adult rat VMs appeared qualitatively similar at day 4 to transduced ARVMs, although TT power was 50 % smaller on average in transduced rat VMs than in transduced ARVMs. This may indicate that TT loss is more complete by day 4 in rat VMs in short-term culture than in ARVMs but could also be due to isolation-dependent variability, particularly as only one rat was used. Crucially, as for ARVMs, the difference in TT power between day 4 GFP+ and JPH2+ rat VMs did not reach statistical significance (cf, Fig. 16 with Fig. 21), again seeming to support the idea that JPH2 overexpression did not prevent or help mitigate loss of TTs in short-term culture. Before reaching this conclusion however, it was essential to first quantify JPH2 staining intensity in rat VMs and verify the efficacy of transduction with the JPH2 construct. Overall, JPH2 staining intensity in transduced rat VMs was approximately 20 % greater on average than in transduced ARVMs (cf, Fig. 21 with Fig. 18) and importantly, where JPH2+ ARVMs had 26 % greater JPH2 staining intensity than GFP+ ARVMs, the difference between rat GFP+ and JPH2+ VMs did not reach statistical significance.

Given the small sample sizes in rat VMs, these data should be interpreted with caution. However, they seem to support the view that there is no obvious species-dependent difference in terms of both TT power and JPH2 staining intensity between JPH2+ adult rabbit and rat ventricular myocytes at day 4 of culture under the experimental conditions used here. With this being said, the observed lack of difference in JPH2 staining intensity between transduced rat cells strongly suggests that overexpression of JPH2 was either unsuccessful or, like in ARVMs, very small. Whether a species difference would manifest in data from recordings taken using conditions where exogenous JPH2 was much more significantly overexpressed is a question that remains.

4.8 Conclusions and Limitations

In JPH2+ ARVMs cultured for four days there was both an absence of TTs indicated by WGA staining and lack of a significant difference in TT power compared to the negative control (GFP+) group. This was surprising, as these data are very disparate from recent similar studies in adult rat VMs and cat VMs (Poulet et al., 2021, Gross et al., 2021). Staining using two different membrane dyes helped to eliminate the idea that the lack of difference in TT power at day 4 between transduced ARVMs was dye-dependent or was a result of some factor during the fixation process. Superficially, transduction did not seem to be an issue as cells were clearly showing GFP fluorescence, however JPH2 staining intensity was only slightly increased in JPH2+ ARVMs. This was very surprising as the data from Mizuguchi et al., (2000) suggest that one can expect proportionality of expression in a bicistronic vector and, furthermore, it has been shown that even in polycistronic vectors with multiple IRES elements (including a GFP reporter) that there is no significant change in expression of the primary transgene (Bouabe et al., 2008). This suggests that something fundamental to JPH2 overexpression was not working as anticipated – and given that GFP was abundantly evident in ARVMs from at least one animal, it is likely that the problem was not with viral transduction but with translation of the JPH2 transgene. As antibody staining only gives an indication of protein expression, and not mRNA, it is not possible to directly tell whether this issue originates with transcription or translation of JPH2. Ideally, a secondary-only antibody control would have been carried out in this work to confirm that background fluorescence was not a confounding variable (for example, in Figure 17, it is possible that some of the fluorescence at day 4 is due to non-specific binding). Furthermore, it would be interesting to quantify this primary antibody's selectivity for JPH2 in a knockout animal model.

The selectivity of this antibody has previously been demonstrated (Kong et al., 2019), and the difference in day 0 and day 4 JPH2 staining intensity in non-transduced cells in the present study supports the view that JPH2 staining was representative of JPH2 distribution. This antibody can detect JPH2 in Western blot (Kong et al., 2019), where protein is linearised – which argues against the idea of a misfolding/trafficking issue (i.e., the JPH2 antibody only recognising a folded epitope), although it remains odd that transduced cells displayed a punctate JPH2 staining profile. The lack of a secondary control for JPH2 staining here may mean that (if background staining was significant) the observed significant differences in

staining intensity between days 0 and 4 in culture and between GFP+ and JPH2+ ARVMs are much greater in terms of percentage change than indicated here.

Testing the JPH2 adenovirus against the negative control (GFP) adenovirus in adult rat VMs using the same experimental conditions again showed that there was no difference in TT power; and, in this smaller sample study, there was also no difference in JPH2 staining. The fact that JPH2 staining intensity was only slightly increased in JPH2+ ARVMs and not at all in adult rat VMs highlights a key issue in the present study - one that makes it very difficult to address the experimental hypothesis: JPH2 doesn't seem to have been overexpressed to a considerable degree. As the effect size in the experimental group (i.e. JPH2 overexpression) was so small or absent, it is also not realistic to make any species comparisons from the data sample presented here in terms of the effect of JPH2 overexpression in adult rabbit and rat VMs.

It is difficult to conclude that the poor overexpression of JPH2 in the present study was due to a problem with the viral vector or coding sequence of the JPH2 construct without further quantitative analysis. The MOI used in this study could also have been a significant factor in why JPH2 overexpression was presumably so low; however, adenoviruses have been shown to be highly efficient in transducing VMs (Zhou et al., 2000), and one study in ARVMs showed that an MOI of 50 was little different to MOIs of up to 1000 in terms of a functional effect resulting from overexpression of the carboxyl terminus of beta-adrenergic receptor kinase (Drazner et al., 1997), though it is difficult to draw such comparisons between different transgenes and across experimental conditions.

4.9 Future work

Western blotting for JPH2 and GFP in the GFP+ and JPH2+ groups could rule out that there is a problem with the viral vector/coding sequence if GFP protein levels correlate well with JPH2 protein levels. It would be worthwhile doing this for MOIs of 50 and of 200. An alternative way to quantify JPH2 overexpression would be to use a JPH2 vector with the addition of an HA tag and corresponding anti-HA antibody to provide an expression profile of exogenous HA-JPH2 (as performed by Gross et al., (2021) (Gross et al., 2021)). One could compare this with JPH2 antibody staining in these same cells to contrast endogenous and exogenous JPH2 expression. Exploring the limiting factors in terms of JPH2 overexpression in

this study would enable subsequent investigators to confidently test the experimental hypothesis. It may be useful to reevaluate cell membrane capacitance for a given virus and MOI in transduced ARVMs once significant levels of JPH2 expression have been achieved.

In terms of the effect of ISO on non-transduced ARVMs, it may be worthwhile to clarify the relationship between days in culture and $t_{½}$ for the increase in I_{Ca} in response to ISO in ARVMs, which could provide some insight into the changes occurring in short-term culture at the cellular level. One could use shorter sampling intervals or even cell lengthening/shortening measurements to achieve this. In addition, further testing of non-transduced cells against 1 µM ISO would help support or refute the relevance of the observed negative shift in I_{Ca} density-V and how it interacts with days in culture. One might also explore these parameters in JPH2+ ARVMs (when overexpression levels are confirmed to be significantly greater) and make use of beta-2 selective agonists such as zinterol in the presence of a saturating concentration of a non-selective/beta-1-selective beta blocker to identify the role of TT-localised adrenergic signalling (in relation to I_{Ca} density) over days in culture and any interaction with JPH2 expression.

5 References

BATHE-PETERS, M., GMACH, P., BOLTZ, H. H., EINSIEDEL, J., GOTTHARDT, M., HUBNER, H., GMEINER, P., LOHSE, M. J. & ANNIBALE, P. 2021. Visualization of beta-adrenergic receptor dynamics and differential localization in cardiomyocytes. *Proc Natl Acad Sci U S A,* 118**,** e2101119118.

BERS, D. M. 2008. Calcium cycling and signaling in cardiac myocytes. *Annu Rev Physiol,* 70**,** 23-49.

BOND, R. C., CHOISY, S. C., BRYANT, S. M., HANCOX, J. C. & JAMES, A. F. 2020. Ion currents, action potentials, and noradrenergic responses in rat pulmonary vein and left atrial cardiomyocytes. *Physiol Rep,* 8**,** e14432.

BOUABE, H., FASSLER, R. & HEESEMANN, J. 2008. Improvement of reporter activity by IRES-mediated polycistronic reporter system. *Nucleic Acids Res,* 36**,** e28.

BRETTE, F., DESPA, S., BERS, D. M. & ORCHARD, C. H. 2005. Spatiotemporal characteristics of SR Ca(2+) uptake and release in detubulated rat ventricular myocytes. *J Mol Cell Cardiol,* 39**,** 804-812.

BRETTE, F., RODRIGUEZ, P., KOMUKAI, K., COLYER, J. & ORCHARD, C. H. 2004a. beta-adrenergic stimulation restores the Ca transient of ventricular myocytes lacking t-tubules. *J Mol Cell Cardiol,* 36**,** 265-275.

BRETTE, F., SALLE, L. & ORCHARD, C. H. 2004b. Differential modulation of L-type Ca2+ current by SR Ca2+ release at the T-tubules and surface membrane of rat ventricular myocytes. *Circ Res,* 95**,** e1-7.

BRYANT, S. M., KONG, C. H. T., CANNELL, M. B., ORCHARD, C. H. & JAMES, A. F. 2018. Loss of caveolin-3-dependent regulation of ICa in rat ventricular myocytes in heart failure. *Am J Physiol Heart Circ Physiol,* 314**,** H521-H529.

BUGAISKY, L. B. & ZAK, R. 1989. Differentiation of adult rat cardiac myocytes in cell culture. *Circ Res,* 64**,** 493-500.

CANNELL, M. B. & KONG, C. H. 2012. Local control in cardiac E-C coupling. *J Mol Cell Cardiol,* 52**,** 298-303.

CHEN, X., PIACENTINO, V., 3RD, FURUKAWA, S., GOLDMAN, B., MARGULIES, K. B. & HOUSER, S. R. 2002. L-type Ca2+ channel density and regulation are altered in failing human ventricular myocytes and recover after support with mechanical assist devices. *Circ Res,* 91**,** 517-524.

CHUNG, J. H., BIESIADECKI, B. J., ZIOLO, M. T., DAVIS, J. P. & JANSSEN, P. M. 2016. Myofilament Calcium Sensitivity: Role in Regulation of In vivo Cardiac Contraction and Relaxation. *Front Physiol,* 7**,** 562.

CROCINI, C., COPPINI, R., FERRANTINI, C., YAN, P., LOEW, L. M., POGGESI, C., CERBAI, E., PAVONE, F. S. & SACCONI, L. 2016. T-Tubular Electrical Defects Contribute to Blunted beta-Adrenergic Response in Heart Failure. *Int J Mol Sci,* 17**,** 1471.

CROSSMAN, D. J., YOUNG, A. A., RUYGROK, P. N., NASON, G. P., BADDELELY, D., SOELLER, C. & CANNELL, M. B. 2015. T-tubule disease: Relationship between t-tubule organization and regional contractile performance in human dilated cardiomyopathy. *J Mol Cell Cardiol,* 84**,** 170-178.

DE LA MATA, A., TAJADA, S., O'DWYER, S., MATSUMOTO, C., DIXON, R. E., HARIHARAN, N., MORENO, C. M. & SANTANA, L. F. 2019. BIN1 Induces the Formation of T-Tubules and Adult-Like Ca(2+) Release Units in Developing Cardiomyocytes. *Stem Cells,* 37**,** 54-64.

DIBB, K. M., LOUCH, W. E. & TRAFFORD, A. W. 2022. Cardiac Transverse Tubules in Physiology and Heart Failure. *Annu Rev Physiol,* 84**,** 229-255.

DRAZNER, M. H., PEPPEL, K. C., DYER, S., GRANT, A. O., KOCH, W. J. & LEFKOWITZ, R. J. 1997. Potentiation of beta-adrenergic signaling by adenoviral-mediated gene transfer in adult rabbit ventricular myocytes. *J Clin Invest,* 99**,** 288-296.

FAWCETT, D. W. & MCNUTT, N. S. 1969. The ultrastructure of the cat myocardium. I. Ventricular papillary muscle. *J Cell Biol,* 42**,** 1-45.

FODERO, L. R., SAEZ-VALERO, J., BARQUERO, M. S., MARCOS, A., MCLEAN, C. A. & SMALL, D. H. 2001. Wheat germ agglutinin-binding glycoproteins are decreased in Alzheimer's disease cerebrospinal fluid. *J Neurochem,* 79**,** 1022-1026.

FOWLER, E. D., KONG, C. H. T., HANCOX, J. C. & CANNELL, M. B. 2018. Late Ca(2+) Sparks and Ripples During the Systolic Ca(2+) Transient in Heart Muscle Cells. *Circ Res,* 122**,** 473-478.

GORELIK, J., WRIGHT, P. T., LYON, A. R. & HARDING, S. E. 2013. Spatial control of the betaAR system in heart failure: the transverse tubule and beyond. *Cardiovasc Res,* 98**,** 216-224.

GROSS, P., JOHNSON, J., ROMERO, C. M., EATON, D. M., POULET, C., SANCHEZ-ALONSO, J., LUCARELLI, C., ROSS, J., GIBB, A. A., GARBINCIUS, J. F., LAMBERT, J., VAROL, E., YANG, Y., WALLNER, M., FELDSOTT, E. A., KUBO, H., BERRETTA, R. M., YU, D., RIZZO, V., ELROD, J., SABRI, A., GORELIK, J., CHEN, X. & HOUSER, S. R. 2021. Interaction of the Joining Region in Junctophilin-2 With the L-Type Ca(2+) Channel Is Pivotal for Cardiac Dyad Assembly and Intracellular Ca(2+) Dynamics. *Circ Res,* 128**,** 92-114.

GUO, A., ZHANG, C., WEI, S., CHEN, B. & SONG, L. S. 2013. Emerging mechanisms of T-tubule remodelling in heart failure. *Cardiovasc Res,* 98**,** 204-215.

HONG, T. & SHAW, R. M. 2017. Cardiac T-Tubule Microanatomy and Function. *Physiol Rev,* 97**,** 227-252.

HONG, T., YANG, H., ZHANG, S. S., CHO, H. C., KALASHNIKOVA, M., SUN, B., ZHANG, H., BHARGAVA, A., GRABE, M., OLGIN, J., GORELIK, J., MARBAN, E., JAN, L. Y. & SHAW, R. M. 2014. Cardiac BIN1 folds T-tubule membrane, controlling ion flux and limiting arrhythmia. *Nat Med,* 20**,** 624-632.

HORACKOVA, M. & BYCZKO, Z. 1997. Differences in the structural characteristics of adult guinea pig and rat cardiomyocytes during their adaptation and maintenance in long-term cultures: confocal microscopy study. *Exp Cell Res,* 237**,** 158-175.

JIANG, M., ZHANG, M., HOWREN, M., WANG, Y., TAN, A., BALIJEPALLI, R. C., HUIZAR, J. F. & TSENG, G. N. 2016. JPH-2 interacts with Cai-handling proteins and ion channels in dyads: Contribution to premature ventricular contraction-induced cardiomyopathy. *Heart Rhythm,* 13**,** 743-752.

JONES, P. P., MACQUAIDE, N. & LOUCH, W. E. 2018. Dyadic Plasticity in Cardiomyocytes. *Front Physiol,* 9**,** 1773.

KAMEYAMA, M., HOFMANN, F. & TRAUTWEIN, W. 1985. On the mechanism of beta-adrenergic regulation of the Ca channel in the guinea-pig heart. *Pflugers Arch,* 405**,** 285-293.

KONG, C. H. T., BRYANT, S. M., WATSON, J. J., GADEBERG, H. C., ROTH, D. M., PATEL, H. H., CANNELL, M. B., ORCHARD, C. H. & JAMES, A. F. 2018a. The Effects of Aging on the Regulation of T-Tubular ICa by Caveolin in Mouse Ventricular Myocytes. *J Gerontol A Biol Sci Med Sci,* 73**,** 711-719.

KONG, C. H. T., BRYANT, S. M., WATSON, J. J., ROTH, D. M., PATEL, H. H., CANNELL, M. B., JAMES, A. F. & ORCHARD, C. H. 2019. Cardiac-specific overexpression of caveolin-3 preserves t-tubular ICa during heart failure in mice. *Exp Physiol,* 104**,** 654-666.

KONG, C. H. T., ROG-ZIELINSKA, E. A., KOHL, P., ORCHARD, C. H. & CANNELL, M. B. 2018b. Solute movement in the t-tubule system of rabbit and mouse cardiomyocytes. *Proc Natl Acad Sci U S A,* 115**,** E7073-E7080.

LEHNART, S.E & WEHRENS, X. H. T. 2022. The role of junctophillin proteins in cellular function. *Physiol Rev*, 2022 Vol. 102, 1211-1261.

LEMERLE, E., LAINE, J., BENOIST, M., MOULAY, G., BIGOT, A., LABASSE, C., MADELAINE, A., CANETTE, A., AUBIN, P., VALLAT, J. M., ROMERO, N. B., BITOUN, M., MOULY, V., MARTY, I., CADOT, B., PICAS, L. & VASSILOPOULOS, S. 2023. Caveolae and Bin1 form ring-shaped platforms for T-tubule initiation. *Elife,* 12**,** e84139.

LEVI, A. J., HANCOX, J. C., HOWARTH, F. C., CROKER, J. & VINNICOMBE, J. 1996. A method for making rapid changes of superfusate whilst maintaining temperature at 37 degrees C. *Pflugers Arch,* 432**,** 930-937.

LIU, C., SPINOZZI, S., CHEN, J. Y., FANG, X., FENG, W., PERKINS, G., CATTANEO, P., GUIMARAES-CAMBOA, N., DALTON, N. D., PETERSON, K. L., WU, T., OUYANG, K., FU, X. D., EVANS, S. M. & CHEN, J. 2019. Nexilin Is a New Component of Junctional Membrane Complexes Required for Cardiac T-Tubule Formation. *Circulation,* 140**,** 55-66.

LIU, G., PAPA, A., KATCHMAN, A. N., ZAKHAROV, S. I., ROYBAL, D., HENNESSEY, J. A., KUSHNER, J., YANG, L., CHEN, B. X., KUSHNIR, A., DANGAS, K., GYGI, S. P., PITT, G. S., COLECRAFT, H. M., BEN-JOHNY, M., KALOCSAY, M. & MARX, S. O. 2020. Mechanism of adrenergic CaV1.2 stimulation revealed by proximity proteomics. *Nature,* 577**,** 695-700.

LOHSE, M. J., ENGELHARDT, S. & ESCHENHAGEN, T. 2003. What is the role of beta-adrenergic signaling in heart failure? *Circ Res,* 93**,** 896-906.

LYU, Y., VERMA, V. K., LEE, Y., TALEB, I., BADOLIA, R., SHANKAR, T. S., KYRIAKOPOULOS, C. P., SELZMAN, C. H., CAINE, W., ALHARETHI, R., NAVANKASATTUSAS, S., SEIDEL, T., DRAKOS, S. G. & SACHSE, F. B. 2021. Remodeling of t-system and proteins underlying excitation-contraction coupling in aging versus failing human heart. *NPJ Aging Mech Dis,* 7**,** 16.

MITCHESON, J. S., HANCOX, J. C. & LEVI, A. J. 1996. Action potentials, ion channel currents and transverse tubule density in adult rabbit ventricular myocytes maintained for 6 days in cell culture. *Pflugers Arch,* 431**,** 814-827.

MITCHESON, J. S., HANCOX, J. C. & LEVI, A. J. 1998. Cultured adult cardiac myocytes: future applications, culture methods, morphological and electrophysiological properties. *Cardiovasc Res,* 39**,** 280-300.

MIZUGUCHI, H., XU, Z., ISHII-WATABE, A., UCHIDA, E. & HAYAKAWA, T. 2000. IRES-dependent second gene expression is significantly lower than cap-dependent first gene expression in a bicistronic vector. *Mol Ther,* 1**,** 376-382.

NIKOLAEV, V. O., MOSHKOV, A., LYON, A. R., MIRAGOLI, M., NOVAK, P., PAUR, H., LOHSE, M. J., KORCHEV, Y. E., HARDING, S. E. & GORELIK, J. 2010. Beta2-adrenergic receptor redistribution in heart failure changes cAMP compartmentation. *Science,* 327**,** 1653-1657.

ORCHARD, C. & BRETTE, F. 2008. T-Tubules and sarcoplasmic reticulum function in cardiac ventricular myocytes. *Cardiovasc Res,* 77**,** 237-244.

ORCHARD, C. H., BRYANT, S. M. & JAMES, A. F. 2013. Do t-tubules play a role in arrhythmogenesis in cardiac ventricular myocytes? *J Physiol,* 591**,** 4141-4147.

OTTOLIA, M., TORRES, N., BRIDGE, J. H., PHILIPSON, K. D. & GOLDHABER, J. I. 2013. Na/Ca exchange and contraction of the heart. *J Mol Cell Cardiol,* 61**,** 28-33.

PABBATHI, V. K., ZHANG, Y. H., MITCHESON, J. S., HINDE, A. K., PERCHENET, L., ARBERRY, L. A., LEVI, A. J. & HANCOX, J. C. 2002. Comparison of Na(+)/Ca(2+) exchanger current and of its response to isoproterenol between acutely isolated and short-term cultured adult ventricular myocytes. *Biochem Biophys Res Commun,* 297**,** 302-308.

PAVLOVIC, D., MCLATCHIE, L. M. & SHATTOCK, M. J. 2010. The rate of loss of T-tubules in cultured adult ventricular myocytes is species dependent. *Exp Physiol,* 95**,** 518-527.

POULET, C., SANCHEZ-ALONSO, J., SWIATLOWSKA, P., MOUY, F., LUCARELLI, C., ALVAREZ-LAVIADA, A., GROSS, P., TERRACCIANO, C., HOUSER, S. & GORELIK, J. 2021. Junctophilin-2 tethers T-tubules and recruits functional L-type calcium channels to lipid rafts in adult cardiomyocytes. *Cardiovasc Res,* 117**,** 149-161.

REYNOLDS, J. O., QUICK, A. P., WANG, Q., BEAVERS, D. L., PHILIPPEN, L. E., SHOWELL, J., BARRETO-TORRES, G., THUERAUF, D. J., DOROUDGAR, S., GLEMBOTSKI, C. C. & WEHRENS, X. H. 2016. Junctophilin-2 gene therapy rescues heart failure by normalizing RyR2-mediated Ca(2+) release. *Int J Cardiol,* 225**,** 371-380.

ROG-ZIELINSKA, E. A., KONG, C. H. T., ZGIERSKI-JOHNSTON, C. M., VERKADE, P., MANTELL, J., CANNELL, M. B. & KOHL, P. 2018. Species differences in the morphology of transverse tubule openings in cardiomyocytes. *Europace,* 20**,** iii120-iii124.

SACCONI, L., FERRANTINI, C., LOTTI, J., COPPINI, R., YAN, P., LOEW, L. M., TESI, C., CERBAI, E., POGGESI, C. & PAVONE, F. S. 2012. Action potential propagation in transverse-axial tubular system is impaired in heart failure. *Proc Natl Acad Sci U S A,* 109**,** 5815-5819.

SANCHEZ-ALONSO, J. L., BHARGAVA, A., O'HARA, T., GLUKHOV, A. V., SCHOBESBERGER, S., BHOGAL, N., SIKKEL, M. B., MANSFIELD, C., KORCHEV, Y. E., LYON, A. R., PUNJABI, P. P., NIKOLAEV, V. O., TRAYANOVA, N. A. & GORELIK, J. 2016. Microdomain-Specific Modulation of L-Type Calcium Channels Leads to Triggered Ventricular Arrhythmia in Heart Failure. *Circ Res,* 119**,** 944-955.

SCHNEIDER, C. A., RASBAND, W. S. & ELICEIRI, K. W. 2012. NIH Image to ImageJ: 25 years of image analysis. *Nat Methods,* 9**,** 671-675.

SETTERBERG, I. E., LE, C., FRISK, M., LI, J. & LOUCH, W. E. 2021. The Physiology and Pathophysiology of T-Tubules in the Heart. *Front Physiol,* 12**,** 718404.

SOELLER, C. & CANNELL, M. B. 1999. Examination of the transverse tubular system in living cardiac rat myocytes by 2-photon microscopy and digital image-processing techniques. *Circ Res,* 84**,** 266-275.

TAKESHIMA, H., HOSHIJIMA, M. & SONG, L. S. 2015. Ca(2)(+) microdomains organized by junctophilins. *Cell Calcium,* 58**,** 349-356.

TIAHO, F., NARGEOT, J. & RICHARD, S. 1991. Voltage-dependent regulation of L-type cardiac Ca channels by isoproterenol. *Pflugers Arch,* 419**,** 596-602.

WEI, S., GUO, A., CHEN, B., KUTSCHKE, W., XIE, Y. P., ZIMMERMAN, K., WEISS, R. M., ANDERSON, M. E., CHENG, H. & SONG, L. S. 2010. T-tubule remodeling during transition from hypertrophy to heart failure. *Circ Res,* 107**,** 520-531.

WOO, A. Y. & XIAO, R. P. 2012. beta-Adrenergic receptor subtype signaling in heart: from bench to bedside. *Acta Pharmacol Sin,* 33**,** 335-541.

WRIGHT, P. T., BHOGAL, N. K., DIAKONOV, I., PANNELL, L. M. K., PERERA, R. K., BORK, N. I., SCHOBESBERGER, S., LUCARELLI, C., FAGGIAN, G., ALVAREZ-LAVIADA, A., ZACCOLO,

M., KAMP, T. J., BALIJEPALLI, R. C., LYON, A. R., HARDING, S. E., NIKOLAEV, V. O. & GORELIK, J. 2018. Cardiomyocyte Membrane Structure and cAMP Compartmentation Produce Anatomical Variation in beta2AR-cAMP Responsiveness in Murine Hearts. *Cell Rep,* 23**,** 459-469.

YANG, L., LI, R. C., XIANG, B., LI, Y. C., WANG, L. P., GUO, Y. B., LIANG, J. H., WANG, X. T., HOU, T., XING, X., ZHOU, Z. Q., YE, H., FENG, R. Q., LAKATTA, E. G., CHAI, Z. & WANG, S. Q. 2021. Transcriptional regulation of intermolecular Ca(2+) signaling in hibernating ground squirrel cardiomyocytes: The myocardin-junctophilin axis. *Proc Natl Acad Sci U S A,* 118**,** e2025333118.

ZHOU, Y. Y., WANG, S. Q., ZHU, W. Z., CHRUSCINSKI, A., KOBILKA, B. K., ZIMAN, B., WANG, S., LAKATTA, E. G., CHENG, H. & XIAO, R. P. 2000. Culture and adenoviral infection of adult mouse cardiac myocytes: methods for cellular genetic physiology. *Am J Physiol Heart Circ Physiol,* 279**,** H429-436.